Transition Metal Alloys of Extraordinary Stability; An Example of Generalized Lewis-Acid-Base Interactions in Metallic Systems

LEO BREWER AND PAUL R. WENGERT

The Engel theory of metals predicts unusually high thermodynamic stability for certain classes of alloys of transition metals for which generalized Lewis-acid-base interactions are possible. To test these predictions, phase equilibria were studied for ternary systems of Zr, C, and the transition metals Re, Ru, Os, Rh, Ir, Pd, Pt, Ag, and Au. Similar literature data for Nb, Ta, Hf, Th, Y, Ce, Er, and Pu with Re, Ru, Rh, Ir, Pt, and Au were evaluated. Thermodynamic data for the carbides of Zr, Hf, Th, Nb, Ta, U, and Y were critically evaluated, tabulated for 1200 to 2300 K, and used to fix the Gibbs energies of formation in kcal/g-atom of alloy, or their limits, for the binary phases of the above metals. In addition, for Zr, activity coefficients and excess Gibbs energies are tabulated. The predicted high stabilities for alloys of Rh, Ir, Pd, and Pt are confirmed with excess Gibbs energies ranging to −100 kcal/g-atom and activity coefficients as low as 10^{-12} for zirconium or hafnium in dilute solutions of platinum at 1800 K. Some of the properties of these unusually stable compounds have been measured.

THE chemical behavior of the elements is determined primarily by the number of valence electrons per atom, the distribution of these electrons among the *s*, *p*, *d*, and *f* subshells, and by the atomic or ionic size. A number of models have been devised to predict chemical behavior from the information on electronic configurations of the elements derived from atomic spectroscopy.[1-4] The present paper will deal with some aspects of the thermodynamics of transition metal alloys. Although size and internal pressure differences play an important role[5] in fixing the Gibbs energy of alloys, it is the purpose of this paper to focus on the role of electronic configurations in fixing the thermodynamic properties of alloys. In particular, we wish to consider alloys in which one of the components is a transition metal with some completely vacant $4d$ or $5d$ orbitals, *e.g.* the *d* orbitals contain less than five *d* electrons, and the other component is a $4d$ or $5d$ transition metal with so many *d* electrons, *e.g.* more than five *d* electrons, that some of the electrons must be paired internally and thus be unavailable for bonding in the pure metal. The Engel correlation[4-12] between crystal structure and electron configuration provides a means of calculating the thermodynamic stability of different crystalline modifications of a metal when spectroscopic data for the gaseous atoms are available[13] or, conversely, spectroscopic data can be calculated[9] when thermodynamic data for the metals are available.

Tungsten metal can be taken as an example of the calculation of the electronic configuration in the metallic state from the spectroscopic data for the gaseous atom. The ground state of gaseous tungsten is the ^5D level of the d^4s^2 configuration.[13] The ^7S level of the d^5s configuration is 8 kcal/mol higher in energy and the ^7F level of the d^4sp configuration is 55 kcal/mol above the ground state.[13] When gaseous tungsten atoms are brought together, the energy of the system will be lowered due to the attractive interaction of some of the valence electrons with the positive charge of the nuclei of the neighboring atoms. The *s* electrons of atoms in the d^4s^2 ground state cannot contribute to this attractive interaction as the completely filled *s* orbitals of adjacent atoms will repel one another. Orbitals that are not completely filled can overlap to allow electrons to bond adjoining nuclei together. The bonding energies for the various types of electrons have been tabulated[6] and one can calculate that the condensation of gaseous tungsten atoms to the metallic state will lower the energy of the d^4s^2 configuration by 136 kcal/mol due to the bonding by four $5d$ electrons. Atoms in the d^5s configuration will be lowered in energy by 211 kcal/mol due to the 157 kcal/mol contribution to the bonding energy by five $5d$ electrons per atom and 54 kcal/mol from the bonding of one $6s$ electron per atom. Atoms in the d^4sp configuration will be lowered in energy by 136 kcal/mol due to the four $5d$ electrons and 107 kcal/mol due to the $6s$ and $6p$ electrons or a total of 243 kcal/mol bonding energy. Because of the different bonding energies for each configuration, the order of the configurations in the metal is different than in the gas. In metallic tungsten, the d^5s configuration is the lowest in energy, a metal with the d^4sp configuration would be 15 kcal/mol higher in energy, and a metal which retained the gaseous ground state configuration d^4s^2 would be 67 kcal/mol higher in energy than the metal with the d^5s configuration.

Calculations of this type to determine the predominant electronic configuration in the solid have been done for each of the transition metals.[6] For most transition metals, the ground state configuration for the gas is the $d^{n-2}s^2$ configuration where *n* is the total number of valence electrons. Due to the unavailability

LEO BREWER is head of Inorganic Materials Research Division and Associate Director, Lawrence Berkeley Laboratory and Professor, Department of Chemistry, University of California, Berkeley, Calif. 94720. PAUL R. WENGERT is Research Engineer, Glass Engineering Research, Owens-Illinois Technical Center, Toledo, Ohio 43601.

Manuscript submitted March 30, 1972.

of the electrons in the closed s^2 orbital for bonding, the ground state $d^{n-2}s^2$ configurations do not drop in energy as much as $d^{n-1}s$, $d^{n-2}sp$, or $d^{n-3}sp^2$ configurations when the atoms are condensed, and the gaseous ground state configuration $d^{n-2}s^2$ is not important for the condensed metal. All of the configurations that are found to be important in the condensed metal have one s electron because of the nonbonding character of the s^2 configuration and the major factor that characterizes the structure and thermodynamics of each metal is the distribution of the remaining valence electrons between the d and p orbitals. For metals such as W, Mo, Cr, Ta, Nb, and V, the bonding energy calculations indicate[6] that the electronic configurations in the metal are close to $d^{n-1}s$ with only small contributions from p electrons. These metals form only the body-centered cubic (bcc) structure at all temperatures and pressures in confirmation of the Engel correlation and the Hume-Rothery rules[4-7] that associate the bcc structure with electronic configurations with one s electron per atom and p electron contributions ranging up to 0.5 p electrons per atom, *e.g.* $sp^{0.5}$. Likewise, it is possible to confirm the Engel correlation of electronic configuration $d^{n-2}sp$ with the occurrence of the hexagonal close-packed (hcp) structure. Spectroscopic data are not yet available to check the Engel correlation of electronic configuration $d^{n-3}sp^2$ with the face-centered cubic close-packed (ccp) structure, but there are ample confirmations[5] of predictions of alloy behavior based on the Engel correlation for the ccp structure to clearly establish that the occurrence of bcc, hcp, or ccp structures depends upon the distribution of electrons between the d and p orbitals.

The bcc structure occurs for low p electron concentrations ranging up to 50 pct of the s electron concentration. The hcp structure is found for intermediate p electron concentrations of the same order as the s electron concentration and the ccp structure is found for even higher p electron to s electron ratios. As the thermodynamic behavior of transition metals and of their alloys depends[5-12] upon the distribution of valence electrons between the d and p orbitals, the determination of the electronic configuration either from gaseous spectroscopic data or from the crystal structure allows one to characterize the thermodynamic behavior. The competition between the d and p electrons determines the particular mix of d and p electrons in the configuration of lowest Gibbs energy for the metal and thus fixes the crystal structure. The s and p electrons, whose orbitals extend beyond nearest neighbors and affect long range order, determine the crystal structure; the particular structure is determined by the ratio of p to s electrons.[5-9] The d electrons, which interact primarily with the nearest neighbors, cannot influence long range order directly, but they fix the crystal structure indirectly by determining the number of p electrons through the competition that fixes the configuration of lowest Gibbs energy.

For increasing p electron concentration, the possible thermodynamically stable crystal structure for transition metal alloys will be found in the sequence:[5] body-centered cubic (bcc) at lowest p concentration, then A15(Cr_3Si), $\sigma(\beta$-U) and related ϕ, δ, P, R, and $D8_5$ structures, $\chi(\alpha$-Mn), $\beta(\beta$-Mn), hexagonal close-packed (hcp) to cubic close-packed (ccp) at highest p concentrations. Suitable size criteria must also be met in addition to the proper range of p electron concentrations. This relationship between the proportion of p electrons among the s, p electrons and the crystal structure has been extensively reviewed.[5-11] It is the purpose of this paper to examine some aspects of the Engel model that relate directly to the unique behavior of d electrons.

There are three properties of d electrons in transition metal alloys that are important in fixing thermodynamic stability:[5-11] 1) d orbital overlap is predominantly with d orbitals of the nearest neighbors; 2) d orbital overlap and bonding is poor, but increases from $3d$ to $4d$ to $5d$ and can be improved by compressing the lattice to decrease the internuclear distance; and 3) d bonding capacity is lost as the number of d electrons per atom is increased from 5 to 10 since the Pauli exclusion principle requires that additional d electrons beyond the half-filled d^5 configuration be paired internally and thus not available for bonding. Two simple examples will be used to illustrate the role of d electron bonding in the prediction of thermodynamic behavior.

The spectroscopic data for gaseous zirconium indicate that two configurations d^3s and d^2sp are of comparable importance in the condensed phase. In agreement with the Engel correlation, zirconium occurs in both the bcc and hcp structures. The bcc structure has the highest entropy due to its lower coordination number and larger vibrational contributions to the entropy and thus is the structure stable at high temperatures.[14] At the start of each transition series, the d orbital is rather extended, but the increase of nuclear charge quickly shrinks the d orbital. For zirconium, the $5s$ and $5p$ orbitals extend out far enough to overlap not only with orbitals of nearest neighbors but with more distant neighbors. The $4d$ orbitals barely extend beyond the filled $4p$ subshell and overlap poorly even with d orbitals of nearest neighbors. For metals of the fourth group and on to the right of the periodic table, the bonding due to the $4d$ electrons is poorer than that due to $5p$ electrons.[6] Decrease of internuclear distance to improve the overlap of d orbitals markedly increases the bonding ability of the $4d$ electrons compared to $5p$ electrons. The compression due to application of pressure will thus stabilize the structure with the most bonding d electrons; the d^3s bcc structure of zirconium will be stabilized with respect to the d^2sp hcp structure by application of pressure. The total number of d electrons per atom decreases in the order bcc > hcp > ccp. Up to the d^5s configuration of the sixth group metals, all of the d electrons are available for bonding; the effect of pressure upon stability is bcc > hcp > ccp for metals on the left hand side of the transition series for which the nuclear charge is large enough to have shrunk the d orbital sufficiently to prevent optimum overlap. Thus the metastable $d^{n-3}sp^2$ ccp structure of Zr, Nb, and Mo would be even less stable under pressure. As there are only five d orbitals, the maximum number of unpaired d electrons available for bonding is five. Each addition of a d electron beyond five forms a pair in a filled orbital which is unavailable for bonding. For Mn, Tc, and Re, the d^5sp hcp structure with five bonding d electrons is predicted to be stabilized by pressure with respect to either the d^6s bcc or d^4sp^2 ccp structure which have only four bonding d electrons. For the other metals of the right hand half of the transition series, the bcc structure has the most d electrons but the few-

est bonding d electrons. For these metals, the effect of pressure upon stability is ccp > hcp > bcc or the reverse of the behavior predicted for the left half of the transition series. These predictions appear to be contrary to thermodynamics in that the order of densities at 1 atm is not always as predicted, but the structures that are predicted to be stabilized by pressure are found to be more compressible and eventually become denser than the competing structure. The predictions of the effect of pressure upon thermodynamic stability that can be made so simply and directly from the Engel correlation have now been confirmed for every example for which complete data exist.[10-12] The enhancement of d electron bonding by reduction of internuclear distance also plays an important role in the stability of the A15(Cr_3Si) phases.[5,11]

The second example of the application of the knowledge of metallic electronic configurations to the prediction of thermodynamic behavior is the prediction of the effect of small additions of alloying metals upon the relative stability of two crystal structures. Again the distribution of electrons between d and p orbitals is decisive. We return to d^3s bcc zirconium in equilibrium with d^2sp hcp zirconium at 1145 K. All transition metals to the right of zirconium have more than 2.5 bonding d electrons. A substitutional replacement of zirconium by a transition metal to the right of zirconium will result in a greater loss of d bonding in hcp zirconium (two bonding d electrons) than in bcc zirconium (three bonding d electrons). In all instances where data are available, these predictions of the effect of alloying upon the relative stabilities of the bcc and hcp structures have been confirmed.[15-17] All transition metals to the right of the fourth group stabilize the bcc structure of Ti, Zr, or Hf relative to the hcp structure whether the pure alloying metal has bcc, hcp, or ccp structure.

The same principles predict that nontransition metals, with no bonding d electrons, in substitutional sites will stabilize the hcp phases of Ti, Zr, and Hf relative to the bcc phase since the phase with the most d bonds per atom will suffer the most upon introduction of atoms with no bonding d orbitals. On the other hand, small atoms such as C, N, or O that can go into interstitial sites will not interfere with d bonding; their principal effect will be their contribution of s and p electrons that will stabilize the close-packed structure over the bcc structure. Examination of the available data[15-17] confirms these predictions. Similar predictions can be made for the effect of alloying upon the phase transformation of Mn, Fe, and Co with equally good confirmation. The same principles have been shown to apply equally well for the lanthanides and actinides.[8,9]

I) LEWIS-ACID-BASE INTERACTIONS

The above introduction has demonstrated how the electronic configuration of a transition metal can be established and how the differences in behavior of electrons in p and d orbitals establishes the thermodynamic response of transition metal systems to pressure changes or small alloying additions. We wish now to extend the ideas presented in the introduction to examine the thermodynamics of systems consisting of metals of the left half of the transition series that have empty d orbitals alloyed with metals of the right half of the transition series that have internally paired d electrons not available for bonding. An example would be d^4s bcc niobium with one empty d orbital alloyed with d^6sp hcp ruthenium with one pair of d electrons not used in bonding. In pure ruthenium, the filled d orbital is nonbonding because it cannot overlap with d orbitals of neighboring ruthenium atoms. An alloy of zirconium and ruthenium provides the possibility of a generalized Lewis-acid-base reaction as illustrated by the classic example of BF_3 with an empty p orbital reacting with the nonbonding pair of electrons of NH_3 or the reaction of gallium with arsenic. Metals such as hafnium and tantalum lack sufficient electrons to use all of their low energy orbitals in bonding and thus do not bond as strongly as tungsten. Likewise metals such as osmium and platinum have too many d electrons resulting in internal pairing of the electrons in filled orbitals which prevents their use in bonding. The use of the empty orbitals of hafnium and tantalum by the nonbonding electrons of osmium and platinum could optimize the use of available orbitals and electrons and approach the high bonding achieved by tungsten.

The quantitative prediction of the enthalpy change for a reaction such as Hf + 3Ir = $HfIr_3$ is very difficult. In d^6sp^2 ccp iridium, each iridium has a pair of electrons that can be donated to each of the three vacant d orbitals in d^2sp hafnium. This would correspond to a formal charge of −3 on the hafnium and +1 on each iridium. An analogous example would be that of $W(CO)_6$ where the six pairs of electrons donated by the CO molecules completely fill all of the d, s, and p orbitals of tungsten and yield a formal charge of −6 on tungsten. It is unreasonable to expect such large actual charges because of polarization of the bonds and because of back bonding through higher energy orbitals. Similar behavior is expected for $HfIr_3$, but the contributions of coulombic bonding due to the small charge difference that might persist, the effect of polarization upon the bond strength, and the effect of backbonding are too difficult to estimate quantitatively. We can predict that there should be a strong interaction between metals like zirconium and hafnium with metals like iridium and platinum; it is not possible to make quantitative predictions without experimental values for some systems to calibrate the contributions of the various interactions listed above. However, it is possible to make some qualitative predictions about the trends to be expected. Since the strength of d electron bonding increases[6] quite markedly from $3d$ to $4d$ and substantially from $4d$ to $5d$, one would predict that the stability of such generalized Lewis-acid-base compounds could be rather small when only $3d$ orbitals are involved, *e.g.* V-Co, and would be largest when only $5d$ orbitals are involved. For a metal A from the left side of the transition series reacting to form an AB_2 or AB_3 phase with B metals ranging from the seventh group, *e.g.* rhenium, to the eleventh group, *e.g.* gold, the stability of the compound is expected to increase as the number of nonbonding d electrons increases to reach a maximum and then decrease as the paired d electrons become so stabilized with increasing nuclear charge that it is difficult to transfer them. Likewise for a given metal B from the right hand side, the variation of A from the sixth to third group is expected to produce an increase in stability of the compound as the number of vacant d orbi-

tals is increased with a subsequent decrease for smaller nuclear charges that could not hold donated electron pairs. For example, for a fifth group metal such as niobium or tantalum, with only one vacant *d* orbital, the interaction to form a NbX_3 or NbX_2 phase would be small with rhenium, would increase substantially with osmium, and would reach a maximum with iridium. For a fourth group metal such as zirconium, with two vacant *d* orbitals, the maximum in stability would shift to the right and should be between iridium and platinum. For a third group metal such as yttrium, the maximum interaction would be expected at platinum. The present work deals with an experimental test of the trends in stability of intermetallic compounds of zirconium that fall in the class of these generalized Lewis-acid-base compounds. The ternary phase diagrams of Zr and C with Re, Ru, Os, Rh, Ir, Pd, Pt, Ag, and Au have been determined in an effort to fix limits on the Gibbs energies of formation of the intermetallic compounds of zirconium. The equilibration of ZrC + C with a ZrM_x alloy provides a simple way of testing the reduction of zirconium activity; the activity of zirconium in the system ZrC + C is $10^{-5.4}$ at 1800 K or $10^{-8.4}$ at 1200 K. The presence of carbon is not expected to modify the properties of the alloy. The Engel theory indicates[5,6] that the solubility of carbon, which is high in metals of the left side of the transition series, will be greatly reduced by addition of metals of the right side with excess electrons that utilize the empty orbitals. With average electron per atom concentrations of over 6.5, the solubility of carbon in the solid alloys should be negligible. A ternary carbide phase was apparently encountered in the Zr-C-Re system, but none of the metals with higher electron concentrations formed ternary carbides.

II) GENERAL EXPERIMENTAL PROCEDURE

To determine the desired ternary phase diagrams, both solid state and liquid state reactions were run. The desired result was to establish the three-phase region involving C and ZrC; the third phase varied from one alloy system to another. The general procedure and equipment are described in Section II. The detailed procedures which varied with each system are given in Section III.

A) Starting Materials

The elemental powders of 200-400 mesh were 99.9 wt pct or higher purity with the exception of Rh (>1 wt pct Ir), Pd (1 wt pct Pt), and Zr. The major impurities of the zirconium powder as reported by the manufacturer were: 0.05 wt pct Fe, 0.1 wt pct O; 0.03 wt pct H; 0.02 wt pct N; <0.02 wt pct Sn; <0.01 wt pct Ti, W, and Zn; and 0.005 wt pct Hf. The ZrC powder was reported by the manufacturer to be 98 wt pct pure, but an independent spectroanalysis showed 0.5 wt pct Hf as the only detectable impurity. The graphite reactant powder was reported to by the manufacturer to be five nines pure. The graphite material used in making the hot press dyes was manufactured by Great Lakes Carbon Company, Sanborn, N.Y., under the trade name of "Graphitite G"; by independent spectroanalysis it was found to contain the following: 0.001 wt pct Cu, ≤0.001 wt pct Ca and Mg; 0.003 wt pct Al; 0.003 wt pct H; 0.006 wt pct O; and 0.001 wt pct N. The additional materials used for the liquid state reactions were silver sponge of 6-14 mesh containing 0.001 wt pct Cu and <0.001 wt pct Ca, and 0.13 mm Au sheet for which analysis showed the major impurities to be 0.02 wt pct Ti, 0.02 wt pct Pd, and 0.015 wt pct Ag. For the Zr-Re binary system, a 3 mm diam rod of zone refined rhenium was used. The powders used for the solid-state reactions and for the alloy synthesis were mixed by rolling.

B) Furnaces Used

Four types of furnaces were used for the equilibrations. A multistation hot press[18] was employed in all solid-state reactions. As the name implies, a sample can be heated and pressed simultaneously. A tantalum filament made from a 25 mm wide and 0.13 mm thick strip and formed into a nearly complete cylinder of 38 mm diam serves as the heating element. The sample dies are fabricated from "Graphitite G". One die consists of two 13 mm diam plungers and a sleeve of 25 mm OD and 13 mm ID. The reactant powders are placed in the die and are hot pressed to a 13 mm diam, 3 mm thick disc. A maximum of eight dies are placed on a lazy susan which can be rotated so that different dies will align with a hydraulic ram used to apply the desired pressure and with the heating assembly. The furnace can be used in vacuum or with any inert atmosphere (0.8 atm Ar was chosen). After one pressing is completed, the pressure is released; the heating assembly is raised; the lazy susan is rotated to the next position; the heating assembly is lowered to surround the second die; and the second hot pressing commences.

A vacuum furnace with a tantalum sheet or a tungsten mesh filament was used for the binary alloy homogenization and for the melting point determinations. Difficulty was encountered in running the hot press for long periods of time and the vacuum furnace was also used to supplement the hot press runs. The samples were initially hot pressed to compact them and to insure that the powder particles were in good contact with each other. Both vacuum and 0.8 atm He were used. The furnace and crucible were baked before runs and the sample weight losses were measured.

An arc furnace with a water-cooled copper crucible was used to initially melt the binary alloys. Thirty g samples of cold pressed powder, or rod in the case of rhenium, were melted into buttons, flipped and remelted five times. A zirconium button was used as a getter to purify the 0.9 atm Ar in the furnace.

An induction furnace was used for the liquid reactions of the silver and gold ternary systems. The crucible made of "Graphitite G" was placed inside a vertical quartz tube. After pumping on the chamber for 2 to 3 h, helium was passed through the tube at 1 atm pressure. A water cooled copper coil surrounding the outside of the quartz tube served as an energy source. Temperature readings were taken with an optical pyrometer. Corrections for furnace windows, reproducibility, and temperature drift are included in the reported data.

C) Methods of Analysis

X-ray diffraction, metallography, and electron probe microanalysis were used to determine the reaction

products. The product phases were identified with a Pickert Model No. 3488K diffractometer. All of the phases observed had been reported previously as indicated in Table VII. Metallography was straightforward; no etching was necessary to produce distinguishable phases.

A Materials Analysis Company Model 400 electron probe microanalyzer was used to determine the concentration of zirconium present in the elemental phases of Re, Ru, Os, Ag, and Au. The accelerating potential selected for the present work was 20 kV. A beam of 1 to 2 μm diam is claimed by the manufacturer. The L_α characteristic X-ray of zirconium at 0.607 nm was detected by a spectrometer using a PET (pentaerythritol) single crystal [(hkl) = (002); $2d$ = 0.8742 nm] and a xenon sealed proportional spectrometer. The specimen current was in the 350 milliamp range. The intensity from a 100 pct pure zirconium standard was on the order of 10,000 to 15,000 counts per 10 s. Data were taken as a group of twenty readings counting for 10 s each or as a group of ten readings counting for 20 s each. The ratio of the sample to standard counts is proportional to the wt pct Zr. The concentration of carbon was not determined. In all of the systems studied, except the C-Zr-Re system, the carbon concentration in the Zr-M phases was assumed to be small. The count from the principal element of the phase, *i.e.*, Re, Ru, Os, Ag, or Au, was monitored by another spectrometer to make sure that there was no interference from the ZrC phase present. The output from the microprobe is automatically fed to a computer key punch and to a typewriter. The computer program used to analyze the data from the microprobe was the EMX-EMX2 combined program written by Frazer, Fitzgerald, and Reid of Scripps Institution of Oceanography.[19] The EMX program corrects for dead-time losses; drift, assuming a linear variation with time; and background. The EMX2 program corrects for absorption by combining the works of Philibert, Duncumb, and Shields, and Henrich. The program corrects for K-K fluorescence but not for K-L or L-L fluorescence because of the uncertainty of such calculations. Since the ZrL_α line of 0.607 nm was used, fluorescence corrections are not applied to this work. No atomic number corrections are included because of the current difficulties with such corrections. The basic program was adapted for use of the Lawrence Berkeley Laboratory CDC 6600 computer.

The error generally attributed to microanalysis using 100 pct standards and computer corrections is ±2 to ±5 pct of the amount of the element.[20-22] The EMX-EMX2 program does not calculate the error of the quantitative analysis given. A Zr-Au test standard was made in the range of the sample concentration to check the microprobe accuracy independent of the assumed accuracy. The test standard was analyzed each time a Zr-Au sample was analyzed. The results are given in Table I. The dates are presented merely to indicate the spread of time over which the readings were taken.

A wet chemical analysis was run to check the microprobe results. The test standard was taken into solution and was compared with solutions of known concentration near the concentration of the microprobe test standard. The actual analysis performed by Robert D. Giaque was by X-ray spectrometry using an iodine-125 radioisotope source and a rhodium target. A complete description of the technique appears elsewhere.[23] The analysis showed that the microprobe test standard contained 3.40 ± 0.07 at. pct Zr.

From Table I, it can be seen that a 26 pct spread in the concentration of zirconium (from 3.0 to 3.8 at. pct Zr in the gold phase) exists in the microprobe data. The spread was attributed to lack of reproducibility at this concentration level and not to sample inhomogeneity which can be determined by noting the spread in the microprobe readings on a given sample at a given time. If one analysis of the microprobe were relied upon, the expected error would be ±13 pct of the actual at. pct Zr at this level of zirconium concentration. Referring to Table I, it can be seen that 50 pct of the analyses are within ±5 pct accuracy. The 80 pct confidence limit of detection given by deBen[24] occurs at 0.076 at. pct Zr. The at. pct Zr found in the test standard at only 50 pct confidence is well above this value.

In summary, the above analysis shows that the present work associated with Zr-Au samples in the 3 at. pct Zr range is in error by ±13 pct of the actual value. The results of the study of the $Zr_{3.40}Au_{96.60}$ test standard showed that an error of ±5 pct cannot be automatically assumed and that making test standards in the composition range of the alloy system of interest is a necessary step if quantitative analysis is desired.

Although the microprobe analyses have a considerable range of uncertainty, the results are sufficiently accurate for the purpose of fixing Gibbs energies of formation of intermetallic phases as illustrated in Appendix B. Even an uncertainty as large as a factor of two in the zirconium concentration produces an uncertainty of only 2.5 kcal/g-atom in the partial molal Gibbs energy of zirconium and there is no difficulty in fixing the trends for values that range from −10 to −100 kcal/g-atom.

D) Superconductivity Measurements

The following compounds were checked for superconductivity: ZrRu, ZrO_2, $ZrIr_3$, ZrAg, and $ZrAu_3$ + $ZrAu_4$ (two phase sample). The mutual inductance of two coaxial coils containing one of the samples was measured. The change in magnetic susceptibility was observed as a function of temperature. No change was observed between 1.4 and 18 K indicating that the samples were neither superconducting nor ferromagnetic in this temperature range. The method used is covered in detail by Nembach.[25]

III) THE DETERMINATION OF TERNARY PHASE DIAGRAMS

A) The C-Zr-Rh, C-Zr-Ir, C-Zr-Pd, and C-Zr-Pt Systems

One mole of ZrC and three moles of iridium powder were mixed and hot pressed for 15 min at 1860 K and 500 bars pressure. X-ray analysis showed a 50 pct conversion to $ZrIr_3$. Three additional hours showed almost complete reaction and three more hours showed no further change. Although the two phases of $ZrIr_3$ and carbon were probably not in final equilibrium within 3 h, the equilibrium phases had already been formed. Analysis of the ZrRu + 1.2C reaction also verified that a 3 h reaction time was sufficient to observe the products which would exist in equilibrium

Table I. Electron Microprobe Analysis of the $Zr_{3.40}Au_{96.60}$ Standard

At. Pct. Zr.	Date	ST and STD for Zirconium Within 3σ
3.47	8/19/68	yes (2.6σ)
3.48	12/ 5/68	no (3.5σ)
3.77	12/17/68	no (4.6σ)
2.96	1/10/69	yes (2.6σ)
2.96	1/11/69	no (5.5σ)
3.46	1/11/69	no (23 σ)

Table II. Reactions of the C-Zr-Rh, C-Zr-Ir, C-Zr-Pt, and C-Zr-Pd Systems in Hot Press

Reactants	Experimental Parameters	Phase Observed
ZrC + 1 Rh	1850 K, 3 hr 490 bar, vacuum	$ZrRh_3$ + ZrC + C s s w
ZrC + 1.78 Ir	1850 K, 3 hr 490 bar, vacuum	$ZrIr_3$ + ZrC + C + Ir s m w
ZrC + 2 Pd	1650 K, 3 hr 490 bar, 0.8 atm Ar	$ZrPd_3$ + ZrC + C s m
ZrC + 2 Pt	1850 K, 3 hr 490 bar, vacuum	$ZrPt_3$ + ZrC + C s m w

Parameters are Temperature, Time, Applied Ram pressure, and atmospheric pressure. The products were analyzed by X-ray diffraction. The "s", "m", and "w" refer to Strong, medium, and weak intensities of the X-ray pattern. (1.0 bar = 0.987 atm pressure.)

eventually. A 3 h reaction time was, therefore, chosen when only the equilibrium phases were to be determined; longer times were used when the concentrations of the equilibrium phases were desired, as in the C-Zr-Ru system.

Since the ZrM_3 ordered structure is present in the zirconium binary systems with Rh, Pd, and Pt as well as Ir, similar reactions were run and the two phase equilibrium between carbon and the ZrM_3 structure was observed in all cases. Mercuri and Criscione[26] observed similar reactions for ZrC with rhenium and iridium between 1475 and 2475 K.

To fix the three phase regions of the diagrams, samples were made with a surplus of ZrC. The details of the reactions are given in Table II. The iridium phase listed under "Phase Observed" had low intensity peaks after heating and is considered to be unreacted material. The graphite peak at $d = 0.3334$ nm was observed in the rhenium and platinum systems; although not observed by X-ray diffraction in the C-Zr-Ir and C-Zr-Pd systems, graphite was observed by metallographic examination. The balanced reactions are $ZrC + 3M \rightarrow ZrM_3 + C$.

Fig. 1 represents the type of ternary diagram determined. The diagram is simplified in that no attempt has been made to show solubility limits. Those joins directly observed by reaction are indicated by solid lines; for the C-Zr-Ir system, $ZrIr_3$ was found to exist in equilibrium with both carbon and ZrC. It may be recalled from thermodynamics that two joins cannot cross, for there would then be a four phase equilibrium at the join intersection for arbitrary fixed temperatures and pressures. Therefore, compounds to the zirconium-rich side of $ZrIr_3$ must be in equilibrium with ZrC and alloys to the iridium-rich side must be in equilibrium with carbon. These possibilities for the C-Zr-Ir system are indicated in Fig. 1 by the dotted joins. Fig. 1 can also be used to represent the C-Zr-Rh, C-Zr-Pd, and C-Zr-Pt systems. The ZrM_3 alloys of Rh, Pd, and Pt exist in equilibrium with carbon and ZrC as experimentally determined and zirconium alloys of Rh, Pd, and Pt, as well as Ir, to the zirconium-rich side of the ZrM_3 phase exist in equilibrium with ZrC. Compositions in the ccp solid solution region on the M-rich side of the ZrM_3 phase exist in equilibrium with graphite.

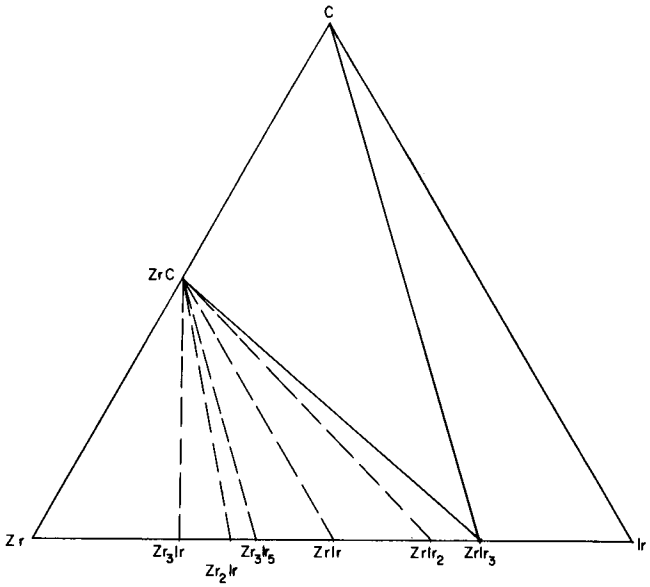

Fig. 1—The C-Zr-Ir ternary phase diagram at around 1800 K. Similar diagrams were established for C-Zr-Rh, C-Zr-Pd, and C-Zr-Pt.

The Gibbs energy of formation of the compounds discussed changes very slowly with changes in temperature and pressure and the corresponding ternary diagrams for all C-Zr-M (M = any of the transition elements Re, Ru, Os, Rh, Ir, Pd, Pt, Ag, or Au) systems may be expected to remain the same throughout the entire solidus region of the diagram, *i.e.*, until the liquid phase is encountered. It is certainly expected to remain the same for the Re, Ru, Os, Rh, Ir, Pd, and Pt systems within several hundred degrees of the range of experimental observations of this work.

Some information was gained on the liquidus phase of the ternary diagrams. A ZrC + 3Ir sample heated to 2275 K melted indicating that the liquidus phase appears below 2275 K but above the 1850 K reaction temperature. Mercuri and Criscione[26] observed the melting of a ZrC + 3Ir sample heated to 2375 K. None of the other samples showed signs of melting at the reaction temperatures listed in Table II. A ZrC + 3Rh sample prepared by Mercuri and Criscione did not melt at 2475 K.

B) Miscellaneous Properties of $ZrIr_3$ and $ZrPt_3$

A separate sample of $ZrIr_3$ was made from the elements and was heated on a tungsten plate in a vacuum furnace. Its observed melting point is 2400 ± 130 K.

An attempt was made to etch the pure $ZrIr_3$ sample. Among the stronger treatments were: boiling in aqua regia for 1.5 h; boiling in concentrated HF for 1.5 h; boiling in a solution of aqua regia and concentrated HF

Table III. Reactions of the C-Zr-Ru, C-Zr-Os and C-Zr-Re Systems in Hot Press

Reactants	Experimental Parameters	Phase Observed
xC + ZrC + 7 Ru	1770 ± 10 K, 7 h 200 bars, 0.8 atm Ar	ZrC + C + Ru (0.20 at. pct Zr)
xC + ZrC + 7 Ru	The above heating plus 1770 ± 10 K, 123 h No applied pressure, 0.8 atm He	ZrC + C + Ru (0.74 at. pct Zr)
1.2 C + ZrRu	1770 K, 3 h 200 bars, 0.8 atm Ar	ZrC + C + $ZrRu_2$ + Ru
1.2 C + ZrRu	The above heating plus 1770 K, 4 h No applied pressure, 0.8 atm He	ZrC + C + Ru*
1.2 C + ZrRu	The above two heatings plus 1770 K, 81 h No applied pressure, 0.8 atm He	ZrC + C + Ru (0.76 at. pct Zr)
$ZrOs_2$ + 1.1 C	1750 K, 12 h 175 bar, 0.8 atm Ar + 1750 K, 2 h 375 bar, 0.8 atm A	C + ZrC + Os*
$ZrOs_2$ + 1.1 C	The above heating plus 1760 K, 140 h No applied pressure, 0.8 atm He	C + ZrC + Os (0.24 at. pct Zr)†
xC + ZrC + 7 Os (0.62 at. pct Zr)	1770 ± 5 K, 120 h 0.8 atm He	ZrC + C + Os (≤0.059 at. pct Zr)
Zr_5Re_{24} + 5.5 C	1770 K, 72 h 350 bar, 0.8 atm Ar	C + Re (16.6 at. pct Zr)
3.6 C + 1.5 ZrC + 1.0 Zr_5Re_{24}	1760 ± 40 K, 96 h 350 bar, 0.8 atm Ar	C + ZrC + Re (19.0 at. pct Zr)

*Although X-ray analysis indicated that the equilibrium phases existed, metallographic examination showed that the phases were too small to be analyzed by the electron probe microanalysis. Further heating promoted grain growth.

†This value was interpreted as interference from the ZrC phase and was not considered.

The Experimental Parameters are temperature, time, applied ram pressure, and atmospheric pressure. The products were analyzed with an electron probe microanalyzer; the obtained Zirconium concentrations are given.

for 0.5 h; heating in molten KOH for 1.5 h. All of these chemical reagents left the sample's shiny metallographically polished surface unattacked. Heating the sample in an air furnace at 1275 K for 0.5 h caused the surface to ripple slightly as if the sample were being annealed. The polished surface still was shiny; no oxide buildup was visible.

$ZrIr_3$ was not found to be superconducting between 1.4 and 18 K. $ZrIr_3$ is brittle and is easily ground.

C) The C-Zr-Ru and C-Zr-Os Systems

Table III summarizes the reactions of the C-Zr-Ru and C-Zr-Os systems. Heating one mole of ZrC, 7 mole of ruthenium, and an unmeasured amount of graphite for a total of 130 h and heating 1 mole of carbon and 1 mole of ZrRu for a total of 88 h indicated that carbon, ZrC, and ruthenium (0.75 pct at. Zr) coexist in equilibrium at 1775 K.

A sample of ruthenium (0.6 at. pct Zr) was made in order to check the microprobe accuracy; however, small inclusions of high zirconium were not homogenized into the ruthenium phase, even after 146 h at 1810 K. The ruthenium phase analyzed as 0.38 at. pct Zr; therefore, the at. pct Zr reading is at least within ±26 pct of the actual value. No correction factor is added to the microprobe results because of the difficulty in getting a good microprobe standard.

The C-Zr-Os system was expected to be analogous to the C-Zr-Ru system. A $ZrOs_2$ alloy was made from elemental powders and hot pressed with graphite in a mole ratio of 1.0 : 1.1 :: $ZrOs_2$: C for 12 h. Although X-ray analysis showed that the reaction was complete with carbon, ZrC, and osmium being the product phases, the osmium grains were too small to obtain unambiguous at. pct Zr microprobe readings from the osmium phase without interference from the ZrC phase. An additional heating at 1760 K for 140 h did not promote sufficiently large grain growth.

In both the ZrRu + 1.2C sample and the $ZrOs_2$ + 1.1C sample, the elemental grain size posed a problem. Although the microprobe's concentrated beam is 1 to 2 micrometers (μm) in diameter, the sample area generating X-rays is larger than expected,[27] possibly 5 to 10 μm in diameter. As a result, a small inclusion of 2 μm diam can be detected but not quantitatively analyzed. Also, small inclusions of a second phase can interfere with the quantitative analysis of a large phase. The C-Zr-Ru and C-Zr-Os equilibrations are fine examples of this difficulty. The zirconium counts of the ZrC phase were on the order of 20,000 counts/20 s, and those of the ruthenium phase were 40 counts/20 s; a very small quantity of ZrC can interfere markedly

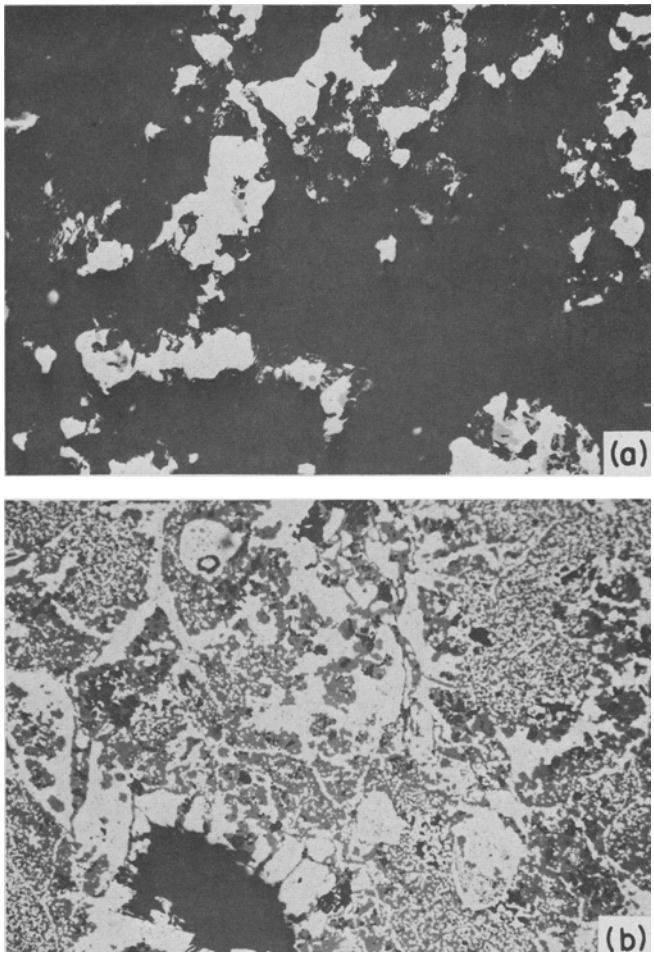

Fig. 2—The C-Zr-Ru system. Magnification 400 times. (*a*) ZrC + 7Ru + *x*C equilibrated for 130 h at 1770 K. (*b*) ZrRu + 1.2C equilibrated for 88 h at 1770 K.

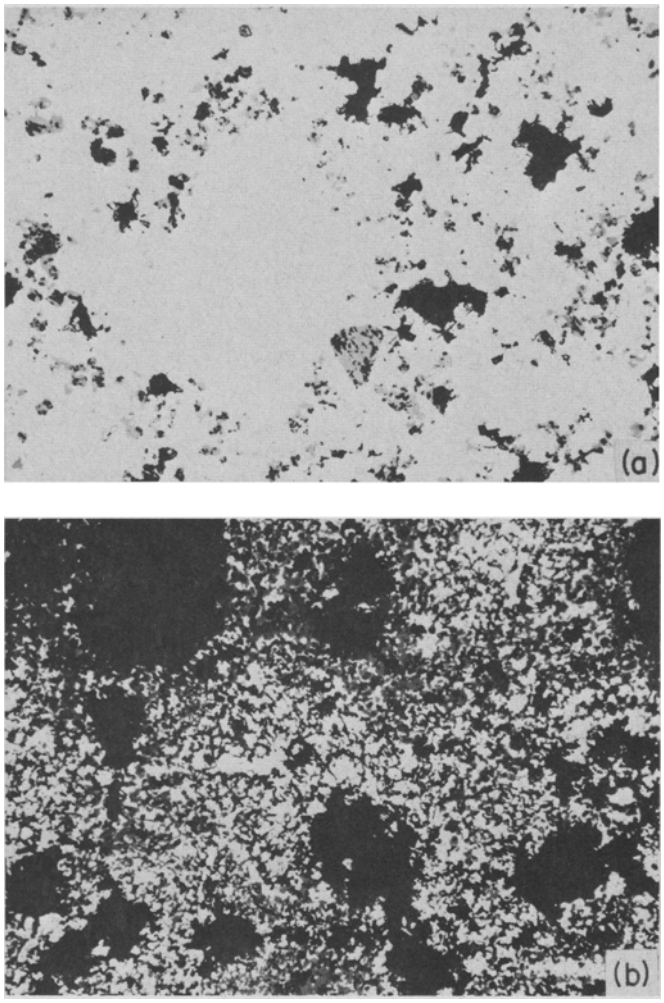

Fig. 3—The C-Zr-Os system. Magnification 400 times. (*a*) ZrC + 7Os + xC equilibrated for 120 h at 1770 K. (*b*) $ZrOs_2$ + 1.1C equilibrated for 154 h at 1760 K.

with the zirconium counts off of the elemental phase. Figs. 2 and 3 are pictures of the metal surfaces at X400, the power of the microscope on the MAC microprobe. When carbon, ZrC, and ruthenium were the reactants, Fig. 2(*a*), the phases were large because there was no phase change and because the reactant powders were large relative to the microprobe beam size. With ZrRu and $ZrOs_2$ as initial phases, Figs. 2(*b*) and 3(*b*), the ZrC, Ru, and Os phases had to nucleate and grow; therefore, their size is much smaller and the ZrC phase is dispersed throughout.

Unlike the $ZrOs_2$ + 1.1C sample, the ZrRu + 1.2C sample gave satisfactory analyses in agreement with the other C-Zr-Ru sample. In order to avoid any ambiguity in the C-Zr-Os system, a sample of ZrC + 7Os + xC (an unmeasured amount of graphite) was made from powder, mixed, and hot-pressed at 2145 K for 17.25 h. Microprobe analysis indicated that 0.62 at. pct Zr had dissolved into the osmium phase. Heating the sample for 120 h at 1770 K left such a low level of zirconium in the osmium phase that it could not be detected by the electron microprobe. In both of the ZrC + 7Os + xC samples, the probe microanalysis of the sample was straightforward; the grain size of the osmium phase was large with no small inclusions of ZrC. Fig. 3(*a*) shows the sample after the 5 d heating at 1770 K.

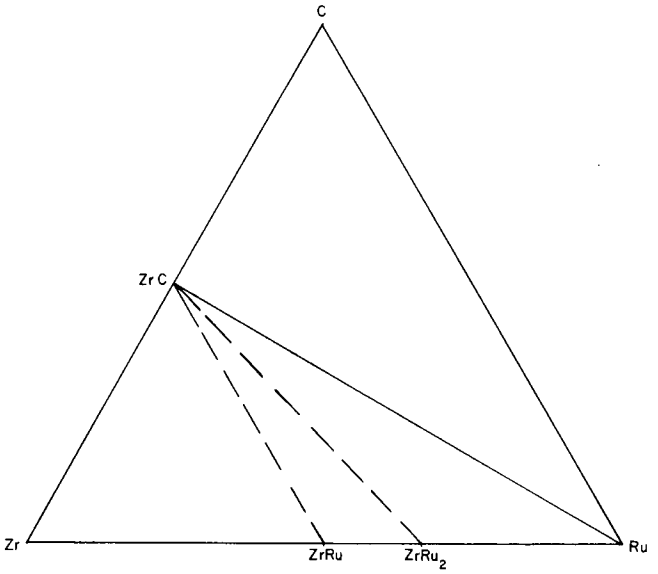

Fig. 4—The C-Zr-Ru ternary phase diagram at around 1800 K. Similar diagrams were established for C-Zr-Os, C-Zr-Ag, and C-Zr-Au. Rhenium also forms a composition triangle with ZrC and carbon, but there also appears to be a ternary carbide phase in the system.

The elemental phases in Figs. 2 and 3 appear as white and the ZrC phase appears as gray. The black areas represent chunks pulled out of the sample due to the interlacing of the relatively weak graphite phase and due to porosity.

In order to determine the detection limit of the microprobe, the formula presented by deBen[24] is used:

$$C_{DL} = \frac{1.47\sqrt{\bar{N}_b}}{\bar{N}_s - \bar{N}_b} C_s$$

where C_{DL} = concentration at the limit of detection of the microprobe (80 pct confidence); $\bar{N}_b$ = average background counts per unit time; $\bar{N}_s$ = average sample counts per unit time; and C_s = concentration of the standard used. It has been stated earlier that this equation cannot be used to assign an error limit to the microprobe readings; that is, if the microprobe analysis of a sample gives a concentration of an element equal to C_{DL} calculated from the equation, then the analysis cannot be assigned a confidence limit of 80 pct automatically. The equation can be used, however, to determine the detection limit of the microprobe since the zirconium background counts from the pure osmium standard were identical to the zirconium counts from the osmium phase of the sample. Using the appropriate values for the C + ZrC + Os sample,

$$C_{DL} = [1.47\sqrt{34}/(30{,}492 - 34)]\ (100\ \text{pct})$$

$$= 0.028\ \text{wt pct Zr or } 0.059\ \text{at. pct Zr}$$

The above calculations show that when the carbon, the ZrC and the osmium phases exist in equilibrium at 1775 K, the concentration of zirconium in the osmium phase is less than 0.06 at. pct Zr.

The resultant C-Zr-Ru and C-Zr-Os ternary phase diagrams are indicated in Fig. 4. The three phase equilibrium between C, ZrC, and Ru (0.75 at. pct Zr) and between C, ZrC, and Os (<0.06 at. pct Zr) was directly observed and is indicated by the solid join between ZrC and ruthenium. The C-Ru solid join corresponds to a side of the diagram. The dashed joins

indicate additional pairs of phases which coexist in equilibrium to avoid crossing of joins as pointed out in the discussion of the C-Zr-Ir system.

Some of the samples gave information on the liquidus phase in the ternary system. A sample of ZrC + 7Ru + 3.2C heated in a graphite crucible to 2145 K had melted while the ZrC + Ru + C samples heated to 1775 K did not melt. A Zr_7Ru_{93} alloy consisting of the ruthenium and the $ZrRu_2$ phases fused to a ZrC crucible at 1970 K; the liquid phase was not encountered when the Zr_7Ru_{93} sample was heated in a ZrC crucible to 1790 K for 141 h. When a $ZrOs_2$ sample was heated in a ZrC crucible to 2750 K, it melted at the point of contact with the crucible. A sample heated to 2290 K did not melt.

D) The Zr-Ru and Zr-Os Binary Systems

A sample of $Zr_{7.5}Ru_{92.5}$ was made from elemental powders, annealed for 141 h at 1790 ± 80 K, and quenched. Metallographic analysis showed two phases were present; X-ray diffraction identified them as ruthenium and $ZrRu_2$. Electron microprobe analysis indicated that 1.15 at. pct Zr in the ruthenium phase exists in equilibrium with the $ZrRu_2$ phase at 1790 ± 80 K.

A $Zr_{1.4}Os_{98.6}$ alloy was arc melted and was homogenized for 13.5 h at 1800 ± 65 K. Metallographic analysis indicated that two phases existed. The large osmium phase was analyzed with the microprobe and found to have a zirconium concentration less than the detection limit of the microprobe, <0.06 at. pct Zr.

The melting points of ZrRu and $ZrOs_2$ were measured to be 2400 ± 70 K and 2845 ± 80 K, respectively. Both compounds are brittle and exhibit no superconductive or ferromagnetic transformation between 1.4 and 18 K.

E) The C-Zr-Re System

Since the ruthenium and osmium phases exist in equilibrium with ZrC and carbon, it was expected that the rhenium phase might also exist in equilibrium with ZrC and carbon and that any compounds of zirconium and rhenium would react with carbon.

The Zr_5Re_{24} phase, the most rhenium-rich phase of the Zr-Re system, is reported[28] to have a composition range of not more than 5 at. pct Zr. A rhenium zone-refined rod and cold pressed zirconium powder were used to make an alloy of 16.6 at. pct Zr as determined by accurate weighing of the original materials. Arc melting the sample was complicated by the fact that stresses were built up in the sample as it cooled after melting. After flipping the sample, initial heating with the arc made the sample fly apart. The Zr_5Re_{24} was annealed for 2 h at 2270 ± 70 K in a vacuum of 10^{-8} atm. Helium (0.8 atm) was added to the furnace at the end of the heating and the sample cooled to ~1020 K in about 8 min. Microprobe analysis indicated that the sample was homogeneous and that it contained 17.5 at. pct Zr. The 5 pct error between the microprobe readings and the original weighing is within the expected accuracy.[20-22] The Zr_5Re_{24} alloy was used as a test standard for the microprobe readings of the rhenium phase of the ternary C-Zr-Re system. The microprobe values are multiplied by 0.95, equal to 16.6/17.5, as a correction factor; but the ±5 error is retained as an expected accuracy.

A portion of the Zr_5Re_{24} compound was ground finer than 200 mesh and heated with graphite as indicated in Table III. X-ray analysis indicated that the rhenium phase was present, that the Zr_5Re_{24} phase had disappeared, and that the ZrC phase had not appeared. Microprobe analysis indicated that the zirconium concentration had remained unchanged. Since the rhenium phase extends to about 2 at. pct Zr[28] and does not extend to 16.6 at. pct Zr in the binary phase, the resultant rhenium phase must be a ternary phase.

To determine the concentration of zirconium in the rhenium phase in equilibrium with both ZrC and carbon, the second reaction given in Table III was run. Microprobe analysis of this sample indicated that the carbon and the ZrC phases exist in equilibrium with a rhenium phase with a molar ratio of Zr/Re = 19.0/81.0. The pct C is not known. The lattice parameters of the hexagonal structure of the $Zr_{19}Re_{81}$ alloy were found to be a_0 = 0.27810 ± 0.00004 nm and c_0 = 0.44590 ± 0.00008 nm. The computer program used to refine the lattice parameters was written by Williams.[29] The lattice parameters are rather close to those of pure rhenium:[30] a_0 = 0.27600 nm and c_0 = 0.44580 nm. Since a change in zirconium concentration from a high value to a lower value was not experimentally observed, it is possible that the hexagonal phase extends to higher zirconium concentrations.

A ternary compound is not unexpected as Fedorov *et al.*[31] have reported a ternary phase $HfRe_4C$ in equilibrium with rhenium and HfC, but Gorshkova *et al.*[32] recently reported ZrC in equilibrium with rhenium and with all Zr-Re phases and observed no ternary phases. This situation is similar to that for the Nb-Re-C and Ta-Re-C systems where Ordan'yan *et al.*[33] report TaC in equilibrium with rhenium. Kua'ma *et al.*[34] report TaC in equilibrium with rhenium and the compounds of tantalum and niobium with rhenium, but they also report ternary phases in the rhenium-rich field of cast alloys. Gorshkova *et al.*[35] find in equilibrium with NbC and TaC an unknown θ phase with an X-ray pattern similar to that of rhenium but with splittings of some lines and with some extra lines. The niobium and tantalum θ phases are isomorphous. Upon long annealing, NbC + θ and TaC + θ change to NbC + Re and TaC + Re. These results could be explained by a metastable ternary phase or by a ternary phase just to the carbon-poor side of the TaC-Re and NbC-Re joins that reacts with carbon in the annealing furnace to convert θ to rhenium and the corresponding carbide. Because of the similarity of the θ and rhenium X-ray patterns, they may not always have been distinguished. In spite of the complication of the θ phase, it is well established that rhenium cannot displace carbon in ZrC, HfC, NbC, or TaC to produce graphite. Thus all of the rhenium compounds of these metals must have Gibbs energies of formation more positve than those of the carbides.

F) The C-Zr-Ag and C-Zr-Au Systems

As indicated in Table IV(a), the solid-state reactions of the C-Zr-Ag and C-Zr-Au systems did not proceed; X-ray diffraction patterns for the reactants and the products were the same.

Table IV. Reactions of the C-Zr-Ag and C-Zr-Au Systems

Reactants	Experimental Parameters	Phases Observed
	(a) Solid-State Reactions	
ZrC + Ag	1160 K, 8 h 490 bar, 0.8 atm Ar	ZrC + Ag
1.2 C + ZrAg	1120 K, 129.5 h 175 bar, 0.8 atm Ar	C + ZrAg
ZrC + 3 Au	1220 K, 88 h 175 bar, 0.8 atm Ar	ZrC + 3 Au (0.51 at. pct Zr)
C + $ZrAu_3$ + $ZrAu_4$	1200 K, 110 h 86 bar, 0.8 atom Ar	C + $ZrAu_3$ + $ZrAu_4$
	(b) Liquid-State Reactions	
C(s) + ZrC(s) + Ag(ℓ)	1680 K, 15 h 1 atm He	C + ZrC + Ag (<0.050 at. pct Zr)
1.2 C(s) + ZrAg(ℓ)	1770 K, 33 h 1 atm He	C + ZrC + Ag (<0.050 at. pct Zr)
C(s) + ZrC(s) + Au(ℓ)	1770 K, 12.2 h 1 atm He	C + ZrC + Au (0.87 at. pct Zr)
C(s) + $ZrAu_3$ + $ZrAu_4$	1770 K, 30 h 1 atm He	C + ZrC + Au
C(s) + $ZrAu_3$ + $ZrAu_4$	1790 ± 65 K, 11.5 h, 1 atm He and 1790 K, 0.5 h	C + ZrC + Au (9.5 ± 3.5 at. pct Zr)

The C-Zr-Ag (liquid) and C-Zr-Au (liquid) reactions are shown in Table IV(b). Microanalysis of the final silver phase found in both C-Zr-Ag (liquid) reactions indicated that the zirconium concentration was below the detection level of the electron probe. Using the equation from deBen[24] as before:

$$C_{DL} = \frac{1.47\sqrt{\bar{N}_b}}{\bar{N}_s - \bar{N}_b} C_s = \frac{1.47\sqrt{11}}{11{,}581 - 11} (100\%)$$

$$= 0.042 \text{ wt \% Zr} \quad \text{or} \quad 0.050 \text{ at. \% Zr}$$

The analysis shows that when liquid silver is in equilibrium with ZrC and carbon at 1770 K, the concentration of zirconium in the silver phase is less than 0.05 at. pct Zr.

When C, ZrC, and Au were inductively heated to 1680 K, the liquid gold formed a bead on top of the ZrC and carbon powders. This same nonwetting phenomenon was also observed in the C, ZrC, liquid Ag reaction. Microprobe analysis indicated that only 0.87 ± 0.16 at. pct Zr had dissolved into the gold phase, a small amount compared to the other C-Zr-Au reactions.

Some of the $Zr_{3.40}Au_{96.60}$ alloy previously used as a test standard was heated with ZrC and carbon in the induction furnace for 12.3 h at 1780 K. No change in the composition of the alloy was observed by microprobe analysis. As a result, no thermodynamic data were derived from this observation.

A sample of $ZrAu_3$ + $ZrAu_4$ + C was heated inductively for approximately 30 h. X-ray diffraction of the resultant powder indicated that a reaction had occurred; the Au, Zr and C phases were observed. No $ZrAu_4$ phase was evident. Since the sample was still a powder, it could not be mounted for electron microprobe analysis.

In order to obtain a gold phase large enough to be analyzed with the microprobe, a $ZrAu_3$ + $ZrAu_4$ + C sample was heated in the hot press for 111.5 h at 1790 ± 65 K with no applied pressure. The sample was then hot pressed at 350 bars pressure for 0.5 h and cooled. The liquid gold alloy had squeezed out of the hot press and had formed five beads. Electron probe microanalysis of four of the beads indicated that the $ZrAu_4$ and the gold phases were present. The beads had apparently been in a colder part of the furnace (below 1330 K) for the last part of the heating cycle so that the gold phase could reach equilibrium with the $ZrAu_4$ phase; Stolz and Schubert[36] indicate that the $ZrAu_4$ phase is a peritectic compound. Microanalysis showed no concentration gradients within the two phases. By microanalysis the $ZrAu_4$ phase was found to contain 20.5 at. pct Zr. Although analyses of two separate beads were within ±0.3 at. pct Zr of this value, a larger ±5 pct of the amount present (0.05 × 0.205 = ±1.0 at. pct Zr) should be assigned to the uncertainty on the basis of the general experience[20-22] with probe microanalysis at this concentration level. The gold phase was found to contain 7.0 at. pct Zr. The analyses of this phase in four of the beads indicated that the associated error was within the ±18 pct of the amount present (±1.3 at. pct Zr), as suggested by the $Zr_{3.40}Au_{96.60}$ standard sample discussed in Section IIC. Metallographic analysis of three beads of the sample using standard area measuring techniques[37] indicated that 40.0 ± 4.4 vol pct of the sample was $ZrAu_4$. Using the theoretical molar volumes calculated from lattice constant information on gold[30] and $ZrAu_4$,[38] the volume percent was converted to the overall percent of zirconium in the liquid phase at 1770 K: 12.3 ± 1.8 at. pct Zr. The details of this calculation are presented in Appendix B of Ref. 10. One of the beads had such small $ZrAu_4$ and gold phases that they could not be analyzed separately; the microprobe readings of the sample indicated the droplet contained 11 at. pct Zr, a value within the accuracy of the combined probe and metallographic analyses of the other beads.

From the analyses of the four liquid C-Zr-Au samples, the at. pct Zr in the gold phase which exists in equilibrium with the ZrC and carbon phases at 1770 K cannot be given a precise value. Since the at. pct Zr was observed to change from 0 pct to 0.87 ± 0.16 pct and from >20 pct to 12.3 ± 1.8 pct, the equilibrium pct Zr value is obviously between 0.71 and 14.1 at. pct Zr. The samples of pure gold and of Au (3.4 at. pct Zr) did not wet the ZrC and carbon powder reactants; the liquid formed a droplet on top of the powder. The nonwetting behavior of these samples may have presented a kinetic barrier to the reaction. Since the zirconium-rich sample which could not be microprobed still remained as a black powder, the gold alloy phase apparently did wet the ZrC and the carbon powders. In this sample, however, no $ZrAu_4$ could be detected by X-ray diffraction. The $ZrAu_4$ structure is a modified hcp structure and the peaks are less intense than the fcc gold structure; however, 40 vol pct of $ZrAu_4$ relative to the gold phase should have been detected if it were present. From the measurements on this sample, the equilibrium percent zirconium in gold is about 7.0 at. pct Zr.

From all of the experimental observations, the zirconium concentration lies between 7.0 ± 1.3 and 12.3 ± 1.8 at. pct Zr. Averaging these two values and taking into account the associated errors, 9.5 ± 3.5 at. pct Zr in gold exists in equilibrium with carbon and ZrC at 1770 K.

Table V. Thermodynamic Properties of Carbides, kcal/mol

	$\Delta H^\circ_{f,298}$	ΔF°_f 1200 K	1800 K	2300 K	Ref.
$ZrC_{0.98}$	−48.8 ± 0.6	−46.1 ± 0.6	−44.2 ± 0.6	−42.3 ± 0.7	39,40
$HfC_{0.96}$	−57.6 ± 0.6	−55.4 ± 0.6	−54.4 ± 0.6	−53.2 ± 0.7	39,41-43
ThC	−29.6 ± 1.1	−25 ± 2	−21 ± 3		39,43-45
$ThC_{1.91}$	−29.9 ± 1.1	−30 ± 2	−30 ± 3	−29 ± 4	39,43,44
$NbC_{0.5}$	−23.3 ± 0.6	−21.3 ± 0.6	−20.5 ± 0.6	−19.7 ± 1	39
$NbC_{0.98}$	−33.4 ± 1	−32.0 ± 1	−31.7 ± 1	−31.5 ± 1	39
$TaC_{0.5}$	−23.7 ± 0.6	−22.7 ± 1	−22.4 ± 1.5	−22.0 ± 1.5	39
TaC	−35.5 ± 1	−34.9 ± 1	−34.9 ± 1.5	−35.0 ± 1.5	39,43
UC	−23.2 ± 0.7	−25.6 ± 0.9	−25.8 ± 1	−25.5 ± 2	43
$UC_{1.5}$	−24.5 ± 2	−25.7 ± 1	−26.5 ± 2		43
$UC_{1.94}$	−21.5 ± 1.5	−25.2 ± 1.5	−26.6 ± 2	−28.5 ± 3	43
YC_2	−27.8 ± 2	−31.5 ± 2	−34.8 ± 2	−37.5 ± 3	46

IV) THERMODYNAMIC DATA FROM TERNARY PHASE DIAGRAMS

A) Thermodynamic Data for the Binary Carbides

To evaluate limits to the Gibbs energies of intermetallic phases from the equilibria involving carbides, it is necessary to know the Gibbs energies of the binary carbides. Table V tabulates the results of a critical survey of the literature. Most of the equilibria to be evaluated involve a carbide saturated with graphite and the compositions of the higher carbides listed in Table V were chosen to be close to the carbon-rich phase boundary. Storms[39] has reviewed the composition limits of the refractory carbides. For ZrC, he lists $ZrC_{0.97}$ as the boundary at 3120 K and $ZrC_{0.98}$ at 2670 K. The values for $ZrC_{0.98}$ in Table V are based on the enthalpy of formation determined by combustion calorimetry by Baker *et al.*[40] and the high temperature Gibbs energy function tabulated by Storms.[39] For HfC, the boundary is $HfC_{0.97}$ at 3450 K and $HfC_{0.98}$ at 1870 K. Although the enthalpy of combustion by Mah[41] is for the composition $HfC_{0.96}$. it was felt that the change in Gibbs energy from $HfC_{0.96}$ to $HfC_{0.98}$ would be within the experimental uncertainty of the value. Mah's enthalpy of formation was recalculated using the enthalpy of formation of HfO_2 recently determined by Huber and Holley.[42] The high temperature Gibbs energy functions tabulated by Hultgren *et al.*[43] and by Storms[39] are in agreement and were used to obtain the Gibbs energies tabulated in Table V for $HfC_{0.96}$. The values given for the thorium carbides are based on the combustion calorimetric results of Huber *et al.*[44] and a reevaluation of the various data reviewed by Storms,[39] Hultgren *et al.*,[43] and Potter.[45] The composition $ThC_{1.91}$ is close to the carbon-rich boundary; the values at 1800 and 2300 K are given for the cubic γ form and the value at 1200 K is given for the monoclinic α form. Storms[39] lists $NbC_{0.97}$ as the boundary at 3570 K. The values for $NbC_{0.5}$ and $NbC_{0.98}$ in Table V are based on the data compiled by Storms.[39] Storms lists as carbon-rich boundaries $TaC_{0.98}$ at 3670 K, $TaC_{0.99}$ at 2670 K, and very close to $TaC_{1.0}$ at lower temperatures. The data for TaC in Table V are from Storms[39] and Hultgren *et al.*[34] The $TaC_{0.5}$ values are based on estimated high temperature Gibbs energy functions and the ΔH°_{298} was selected from Storms' review.[39] Storms lists the carbon-rich compositions of β-UC_2 as $UC_{1.96}$ at 2720 K and $UC_{1.89}$ at 2040 K. For α-UC_2, he lists $UC_{1.86}$ at 2040 K and $UC_{1.96}$ at 1770 K. The values for $UC_{1.94}$ given in Table V are for the cubic β phase at 2300 K and for the tegragonal α phase at the lower temperature. The 1200 K value is for the metastable phase which can be quenched. All of the thermodynamic values are from Hultgren *et al.*[43] Their 2000 K value for UC has been extrapolated to 2300 K and a slight correction to their $UC_{1.5}$ value at 1200 K was made to be consistent with the phase diagram.[39,43] The values for YC_2 are based on the vaporization studies of Storms.[46] Below 1700 K, the carbon-saturated composition[46] does not exceed C/Y = 2.0. The 1200 K value is for β-YC_2, the higher temperature values are for cubic γ-YC_2.

Table VI. The Activity Coefficient of Zirconium (γ_{Zr}) is Calculated From the Three Phase Equilibria Involving Carbon and ZrC. The Extrapolation to Infinite Dilution Yields γ_{Zr} (0 pct Zr) Which is Also Expressed as the Excess Partial Molar Gibbs Energy of Zirconium in the Limit of 0 pct Zr ($\Delta\bar{F}^{xs}_{Zr}$)

Atomic No. Element	At. Pct Zr	Corresponding $\log_{10}\gamma_{Zr}$	$\log_{10}\gamma_{Zr}$ (0 Pct Zr)	$\Delta\bar{F}^{xs}_{Zr}$ (0 Pct Zr) (kcal/mol of Zr) Calc. at 1800 K
44-Ru	0.75	−3.33	−3.39	−28 ± 3
45-Rh	25.0	−4.76	<−7	<−58
46-Pd	25.0	−4.76	<−7	<−58
47-Ag (liq)	≤0.050	≥−2.2	≥−2.2	≥−18
(solid at 1175 K)	0.17	≥−3.1	≥−3.1	≥−17
75-Re	<0.2	>−1.6	>−1.6	>−13
76-Os	≤0.06	≥−2.1	≥−2.1	≥−17
77-Ir	25.0	−4.7	<−7	<−58
78-Pt	25.0	−4.7	≤−12	≤−99
79-Au (liq)	9.5 ± 3.5	−4.4	−4.0 ± 0.3	−41 ± 2
(solid at 1340 K)	7.3	−6.6	−7.7 ± 0.3	−47 ± 2

B) Calculation of Activity Coefficients and Gibbs Energies of Formation from Ternary Phase Diagrams

Table VI presents activity coefficients of zirconium in alloys of Re, Ru, Os, Rh, Ir, Pd, Pt, Ag, and Au that have been calculated from the ternary phase diagrams represented in Figs. 1 and 4 based on the observations tabulated in Tables II to IV and discussed in Parts A to F of Section III. The activity of zirconium, a_{Zr}, is calculated from values of ΔF°_f(ZrC) in Table V. The activity coefficients of zirconium are calculated by $\gamma_{Zr} = a_{Zr}/X_{Zr}$ based on the pure zirconium standard state and are given in column 3 of Table VI as $\log_{10}\gamma_{Zr}$. The experimentally determined mole fractions, X_{Zr}, are given in column 2 of Table VI; where only limits on X_{Zr} are known, limits on γ_{Zr} are given. To allow ready comparison without need to correct for temperature, the values are presented for 1800 K. As the results for gold and silver at 1800 K are for liquid solutions, values are also given for solid gold and silver at lower temperatures.

Columns 4 and 5 of Table VI present values of $\log\gamma$ (0 pct Zr) and $\Delta\bar{F}^{xs}_{Zr}$ (0 pct Zr) that have been obtained by extrapolation to zero concentration of zirconium by methods given in detail in Part A of the Appendix. These quantities are particularly useful for showing the change in the interaction of zirconium with solvent as a function of electronic composition as indicated by the atomic number. Since the comparison is made in the limit of 0 pct Zr, the effect of composition as a

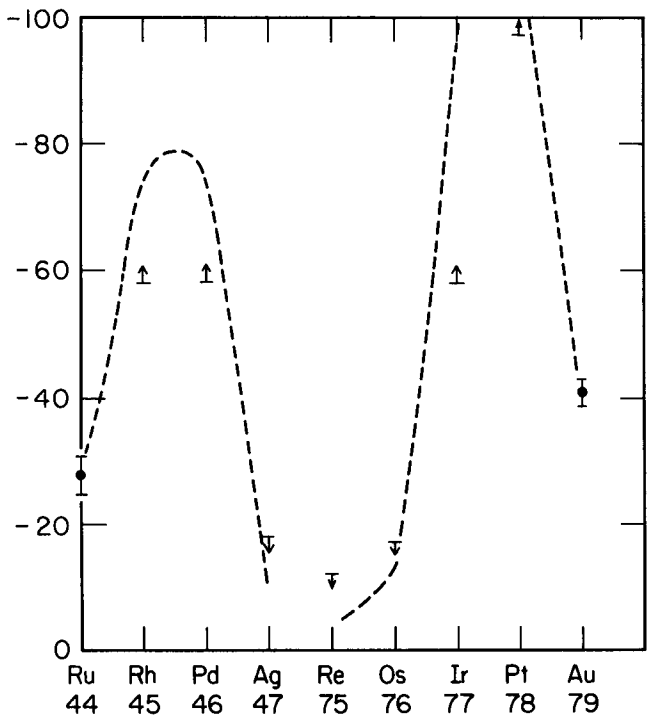

Fig. 5—Excess partial molal Gibbs energy of zirconium in kcal/g-atom at low concentrations in Ru, Rh, Pd, Ag, Re, Os, Ir, Pt, and Au at 1800 K.

variable has been removed. Fig. 5 presents a plot vs atomic number of the solvent of possible $\Delta\bar{F}^{xs}_{Zr}$ values that are consistent with the limits set by the experimental results. A very striking maximum in the interaction of zirconium with metals of the ninth and tenth groups is indicated.

Limits to the integral Gibbs energies of formation of the various binary phases of zirconium were also calculated. In some instances additional data were available to provide closer limits. For example, the formation of $ZrPt_3$ in the reaction of platinum with ZrC at 1800 K fixes ΔF°_f ($ZrPt_3$) as less negative than ΔF°_f (ZrC) = −44.2 kcal/mol. However, Stowe[47] determined ΔF°_f ($ZrPt_3$) ≤ −80 kcal/mol at 1270 K by observing the reaction $ZrO_2 + 3Pt + 2H_2(g) \rightarrow ZrPt_3 + 2H_2O(g)$. ZrO_2 and platinum powders were mixed in the ZrO_2 : Pt molar ratios of 1 : 2, 2 : 3, and 4 : 5 and pressed into pellets 13 by 5 mm. A ZrO_2 blank was also made. Each sample was placed on platinum foil in a nickel boat and heated in a tube furnace. H_2 gas was passed through the furnace for periods of 14 to 17 h. Furnace runs were made at 1070, 1270, and 1420 K. The extent of reaction was measured by the weight loss. A more detailed description of the procedure used can be found in Ref. 10.

Also high temperature solid-electrolyte electromotive force measurements by Worrell and Meschter[48] yield $\log_{10}a_{Zr} = -15.40$ at 1273 K for the two phases $ZrPt_3$ + Zr_9Pt_{41}. Ficalora[49] has burned $ZrPt_3$ in a fluorine calorimeter and preliminary results indicate ΔH°_f ($ZrPt_3$) = −123.5 ± 6 kcal/mol. Carbonara and Blue[50] have measured the partial pressures of ZrO and beryllium in equilibrium with BeO and an alloy richer in platinum than $ZrPt_3$ to obtain $\Delta\bar{F}_{Zr} = -82$ kcal/g-atom at 2200 K.

Mercuri and Criscione[26] have observed the reaction of ZrB_2 with rhodium and iridium to form $ZrRh_3$ and $ZrIr_3$, respectively, together with unidentified phases, probably borides of rhodium and iridium. These reactions set Gibbs energy limits similar to those given by the carbide reactions.

Table VII presents a list of the binary compounds of Zr with Re, Ru, Os, Rh, Ir, Pd, Pt, Ag, and Au with their crystal structures, their melting points, and values of ΔF°_f expressed in kcal/g-atom. Part B of the Appendix presents the details of the calculations of the values of ΔF°_f or limits to those values and describes the ways in which ternary phase equilibria can be used together with binary phase diagrams to fix the Gibbs energies of the phases. The temperature for which the ΔF°_f was evaluated is given, but the values can be used over a wide temperature range as ΔS°_f is close to zero, generally not deviating by more than 1 cal/K g-atom when the compound and the pure elements are all solid.

The Pearson structure nomenclature[51] has been used as described in footnote a of Table VII. A few of the binary phases listed in the literature have been omitted from Table VII. The Zr_3Rh structure (*c*F112, $E9_3$, CFe_3W_3; a = 0.354 nm) reported by Raub and Anderson[52] has been omitted as the structure is common to ternary systems containing C, N, or O and the later works of Zegler[53] and Raman and Schubert[54] did not find this structure. The structure of Zr_2Rh and Zr_2Ir, which has remained undetermined for some time,[54,55] has been determined by Zegler.[53] There is a possibility that high and low temperature forms do exist at this stoichiometry which would explain why the phase was not recognized earlier.[54,55] Raman and Schubert[54] were uncertain of a Zr_3Rh_4 phase (*c*F112, $E9_3$, CFe_3W_3; a = 1.246 nm) and they also reported a $Zr_{45}Rh_{55}$ phase with an undetermined structure; neither of these phases is listed in Table VII. The Ti_2Ni type structure of Zr_2Ir has been shown to definitely contain oxygen[55,56] and only the Al_2Cu type structure is indicated for Zr_2Ir in Table VII. The phase between 33 and 37 at. pct Ir of unknown structure[54] has been omitted. Likewise the Zr_3Ag phase reported by Karlsson[57] as tP4, $L6_0$, $CuTi_3$ (a = 0.4566 nm, c = 0.3986 nm) has been omitted as Betterton and Easton[58] indicate that it does not exist in the binary system. The Zr_2Re phase has been classified[28] as a σ type phase, but it is most likely[5] of the related φHfRe type. Zr_4Pt_5 and Zr_2Pt_{3-} are phases of unknown structure;[54] Zr_2Pt_{3-} would be expected to be of the C11b $MoSi_2$ type or possibly a Laves phase.

The ZrM phases, where M is Os, Ru, Ir, Rh, Pt, and Pd, deserve special comment. Wang[59] has studied ZrRu, ZrRh, and ZrPd and found that ZrRh and ZrPd undergo a martensitic transformation in a manner similar to TiNi. He finds similar behavior for HfIr and HfPt. He suggests that the CsCl structure of ZrRu and HfOs extends to ZrPd and HfPt with increase in the temperature of the martensitic transformation. He was unable to characterize the structure of the low temperature form. Raman and Schubert[54] studied the Zr-Rh, Hf-Rh, Zr-Ir, Hf-Ir, Zr-Pt, and Hf-Pt systems. In most systems, they found a CsCl type structure around the 50 at. pct composition that transformed in a complicated way to several low temperature phases. A phase characterized as the ZrIr type was reported for $ZrRh_{1-}$, HfRh, ZrIr, and HfIr. A phase characterized as the orthorhombic NbRu type was reported for Zr_3Rh_5, $Hf_{42}Rh_{58}$, and $HfIr_{1+}$. The NbRu type is also found[17,54] for $Ti_{45}Rh_{55}$, TiIr, NbRu, and TaRu. It may also occur for NbRh and TaRh at high temperature. It seems likely

Table VII. The Standard Gibbs Energy of Formation (ΔF_f°) of Compounds of the Zirconium Binary Systems

Stoichiometry	Phase Information: Structure: Pearson*; Strukterbericht; Type	References	Melting Point; "p" Implies Peritectic Melting; "c" Implies Congruent Melting	ΔF_f° (kcal/g-atom) Calculated at 1800 K Except When Otherwise Indicated
Zr_2Re	σ type phase [28] but more likely ϕ HfRe type[5] a = 1.012, c = 0.542 nm	5, 16, 17, 28	2170 K p	>−29
$ZrRe_2$	hP12, C14, $MgZn_2$ a = 0.5269, c = 0.8626 nm	16, 17, 28, 51	3020 K c	>−15
Zr_5Re_{24}	cI58, A12, α-Mn a = 0.9693 to 0.9698 nm	16, 17, 28, 51	2770 K p	⩾−7
ZrRu	cP2, B2, CsCl a = 0.3253 nm	17, 51, 59, 71, 72	2370 K c 2400 ± 70 K†	−21.5 ± 1.5 at 1570 K
$ZrRu_2$	hP12, C14, $MgZn_2$ a = 0.5141, c = 0.8509 nm	15, 17, 51, 71-74	2230 ± 50 K p	−14.2 ± 0.9
Zr_7Os_3	tetragonal, ϕ HfRe type	5	–	>−16
ZrOs	cP2, B2, CsCl a = 0.3263 nm	16, 51, 72, 94	2313 K p	⩾−11
$ZrOs_2$	hP12, C14, $MgZn_2$ a = 0.5189, c = 0.8526 nm	16, 51, 73, 77, 94	2840 ± 80 K† 2933 K c	⩾−8
Zr_2Rh	tI12, C16, Al_2Cu a = 0.6440, c = 0.5066 nm	17, 53-55	–	<−5
$ZrRh_{1-}$	ZrIr type	17, 54	–	<−7
$ZrRh_{1+}$	cP2, B2, CsCl (above 650 K)[59]	17, 54, 59	–	<−7
Zr_3Rh_5	NbRu type a = 0.440, b = 0.433, c = 0.342 nm	17, 54	–	<−9
$ZrRh_3$	cP4, L12, $AuCu_3$ a = 0.32927 nm	16, 17, 51, 54, 74	–	<−11 at 1850 K
Zr_3Ir	tP30, $D8_b$, σ or βU a = 1.078, c = 0.5618 nm	17, 51, 54	–	<−4
Zr_2Ir	tI12, C16, Al_2Cu	17, 53-55	–	<−5
Zr_5Ir_3	hP16, $D8_8$, Mn_5Si_3 a = 0.8025, c = 0.5488 nm	17, 53, 54, 76	>1900 K	<−6
ZrIr	ZrIr type	17, 54	>1900 K	<−7
$ZrIr_2$	cF24, C15, $MgCu_2$ a = 0.7359 nm	17, 51, 54, 73, 77	–	<−10
$ZrIr_3$	cP4, $L1_2$, $AuCu_3$ a = 0.3943 nm	17, 51, 74	2400 ± 135 K†	<−11 at 1850 K
Zr_2Pd	tI6, $C11_b$, $MoSi_2$ a = 0.3306, c = 1.0894 nm	16, 17, 36, 51, 79-80, 92	1360 K c	<−5.1 at 1360 K
ZrPd	TiNi type (below M_f)[29] or NbRu type ?	36, 59, 92	>1870 K c	<−7 at 1650 K
$Zr_{44}Pd_{56}$	?	16, 36	–	<−8 at 1650 K
$ZrPd_2$	tI6, $C11_b$, $MoSi_2$ a = 0.3407, c = 0.8597 nm	36, 51, 80, 92	∿1750 K p	<−10 at 1650 K
$ZrPd_3$	hP16, DO_{24}, $TiNi_3$ a = 0.5612, c = 0.9235 nm	36, 51, 74, 92	>1800 K c	<−11 at 1650 K
$ZrPd_4$	CP4, $L1_2$, $AuCu_3$ a = 0.3962 nm	36, 51, 81	–	<−12 at 1650 K
Zr_5Pt_3	hP16, $D8_8$, Mn_5Si_3 a = 0.8201, c = 0.5405 nm	17, 54, 55, 76	2000 K p	<−15
ZrPt	oC8, B_f, ζ−BCr a = 0.3409, b = 1.0315 nm c = 0.4277 nm	17, 51, 54, 82	tr. to B2 at high temperature	<−20
$ZrPt_{1+}$	*cP2*, B2, CsCl a = 0.331 nm	17, 51, 54	2370 K c	<−20
Zr_4Pt_5	?	17, 54	<2270 K p	$-22 \geqslant \Delta F_f^\circ > -52$
Zr_2Pt_{3-}	*tI6*, $C11_b$?	5, 17, 54	<2270 K	$-24 \geqslant \Delta F_f^\circ > -47$
$ZrPt_3$	*hP*16, DO_{24}, $TiNi_3$ a = 0.5645, c = 0.9235 nm	16, 17, 51, 54, 83, 88	2390 to 2470 K c	−30 ± 2
$ZrPt_{3+x}$	cP4, $L1_2$, $AuCu_3$ a = 0.399 nm	84, 88	2270 K p	−27 ± 2

Table VII. (Contd)

Stoichiometry	Phase Information Structure: Pearson*; Strukterbericht; Type	References	Melting Point; "p" Implies Peritectic Melting; "c" Implies Congruent Melting	ΔF_f°(kcal/g-atom) Calculated at 1800 K Except When Otherwise Indicated
$ZrPt_8$	$tI18$, $TiPt_8$ $a = 0.8386$, $c = 0.4027$ nm	85	2120 K	$\leqslant -13$
Zr_2Ag	$tI6$, $C11_b$, $MoSi_2$ $a = 0.32464$, $c = 1.2004$ nm	16, 17, 43, 51, 58, 79	1464 K p	>-20 at 1228 K
ZrAg	tP4, B11, γ-CuTi $a = 0.3468$, $c = 0.6603$ nm	16, 17, 43 51, 58, 86	1410 K c	>-15 at 1228 K
Zr_3Au	cP8, A15, β-W $a = 0.54824$ nm	17, 36, 51, 87	>1270 K p	<-4 at 1370 K
Zr_2Au	tI6, $C11_b$, $MoSi_2$ $a = 0.3272$, $c = 1.150$ nm	17, 36, 51 79	~1370 K p	<-5 at 1370 K
Zr_5Au_4		17, 36	1620 K ? c	<-7 at 1400 K
Zr_7Au_{10}	tI $a = 0.6696$, $c = 1.3292$ nm	17, 36, 51	~1490 K p	<-9 at 1400 K
$ZrAu_2$	$tI6$, $C11_b$, $MoSi_2$ $a = 0.3532$, $c = 0.8718$ nm	17, 36, 51, 56	1690 K p	$-11 \geqslant \Delta F_f^\circ \geqslant -16$ at 1400 K
$ZrAu_3$	orthorhombic, β-Cu_3Ti $a = 0.6062$, $b = 0.4865$, $c = 0.4785$ nm	17, 36, 38, 51	~1830 K c	-12 ± 1 at 1400 K
$ZrAu_4$	oP20 D_{2h}^{16} (*Pnma*)-*Pbnm* orthogonal axes: $5a = 5(0.2858) = 1.4294$, $b = 0.5006$, $c = 0.4845$ nm	17, 36, 38, 51	$\geqslant$1340 K p	-10 ± 0.5 at 1340 K

*Pearson nomenclature was used because of its condensation of much directly readable information. A brief description from Ref. 51 is in order. The first small letter denotes: a = triclinic (anorthic); m = monoclinic; o = orthorhombic; t = tetragonal; h = hexagonal; and c = cubic. The capital letters imply: P = primitive; C = one-face-centered; F = all-face-centered; I = body-centered; R = rhomdehedral. The number following gives the number of atoms in the crystallographic cell.

†These melting points were experimentally observed in the present study; the others are reported in the literature.

The symbols used to represent the structures of Table VII that are given in Figs. 6 and 7 are as follows: I:bcc A2 and ordered cP2, B2, CsCl; II:hcp A3 and ordered hP16, DO_{24}, $TiNi_3$; III:ccp Al and ordered cP4, Ll_2, $AuCu_3$; L:hP12, C14, $MgZn_2$ and cF24, C15, $MgCu_2$; χ:cI58, A12, α-Mn; $C11_b$:tI6, $C11_b$, $MoSi_2$; C16:tI12, C16, Al_2Cu; $D8_8$: hP16, $D8_8$, Mn_5Si_3; B_f:oC8, B_f, ζ-CrB; σ:tP30, $D8_b$, β-U; ϕ:ϕ(HfRe).

that there is an extended CsCl-type composition range at high temperatures that disproportionates to several low temperature phases of slightly different composition ranges. As the equilibrium transformations may be sluggish, martensitic transformations from CsCl to f.c. tetragonal and f.c. orthorhombic phases are observed.

Fig. 6 shows the phase regions of the Zr-(Re, Os, Ir, Pt) diagrams and Fig. 7 shows the phase regions of the Zr-(Tc, Ru, Rh, and Pd) diagrams. These diagrams represent projections along the temperature axis so that the composition ranges indicated for each phase region are the maximum ranges at the optimum temperatures. The abscissa is indicated in atomic percent. For example, the boundaries along the top of Fig. 6 at the level of rhenium indicate that rhenium dissolved in bcc zirconium, represented by I, up to a maximum of 8 at. pct. Then there is a two phase region of I + ϕ phases to 35 at. pct Re. The ϕ phase region with a maximum range of 5 at. pct Re is described in the literature as a σ phase, but it is given in Fig. 6 as the closely related ϕ structure of the Hf-Re system. The phase region from 65 to 70 at. pct Re labelled L corresponds to the $MgZn_2$ type Laves phase. The χ phase region between 80 and 83 at. pct Re corresponds to the $cI58$ α-Mn structure, and finally the II hcp rhenium can dissolve around 1 at. pct Zr. The number after each metal on the right is the number of valence electrons per atom, which is the ordinate. As the elements are adjoining

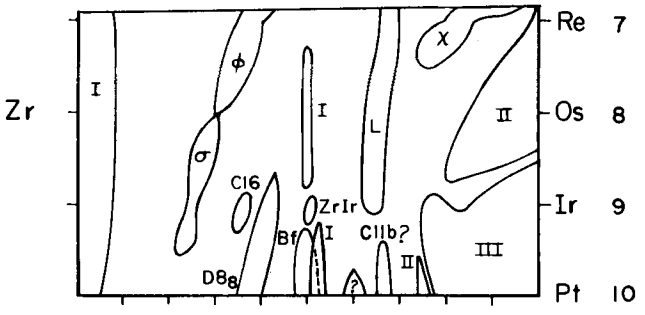

Fig. 6—Phase regions for Zr-(Re, Os, Ir, Pt) projected along temperature axis. Symbols are defined at end of Table VII.

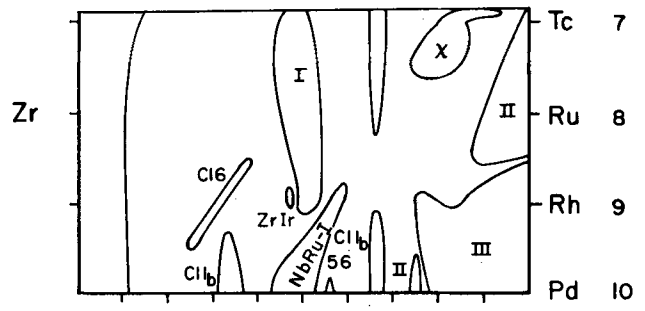

Fig. 7—Phase regions for Zr-(Tc, Ru, Rh, Pd) projected along temperature axis. Symbols are defined at end of Table VII.

metals of the 5*d* period, the phase regions of any of the multicomponent mixtures of these metals with zirco-

Table VIII. Reactions of NbC[60] and TaC[63] with Ru, Ir, and Pt

NbC + Ru	no change	1470 K
NbC + 3 Ir	no change	1470 K
NbC + 3 Ir	→ $NbIr_3$ + C	1770 K
NbC + 3 Pt	→ $NbPt_3$ (α and β) + C	1470 K and 1770 K
TaC + 3 Pt	→ $TaPt_3$ + C	1670 K and 1870 K, 0.5 hr, 600 bars

Table IX. Hf and Th Carbide Reactions with Rh and Ir[26] and Au[61]

Reactants	Experimental Parameters	Phase Observed
HfC + 3 Rh	1270 – 1470 K	$HfRh_3$
HfC + 3 Ir	1500 – 2470 K, 0.5 hr	$HfIr_3$
ThC_2 + 2 Ir	2200 K	$ThIr_2$
ThC_2 + 2 Rh	2170 K (melt) vacuum	?
ThC + 3 Au	1120 K, 114 hr 5×10^{-9} atm	$ThAu_3$ (?)

Table X. Zr and Hf Boride Reactions with Rh and Ir[26]

Reactants	Experimental Parameters	Phases Observed	Minimum Reaction Temperatures, K
ZrB_2 + 4.75 Rh	1700 K, 0.5 hr	$ZrRh_3$ + ?	1470 ± 5
ZrB_2 + 4.75 Ir	1700 K, 0.5 hr	$ZrIr_3$ + ?	1495 ± 5
HfB_2 + 4.75 Rh	1700 K, 0.5 hr	$HfRh_3$ + ?	1440 ± 5
HfB_2 + 4.75 Ir	1700 K, 0.5 hr	$HfIr_3$ + ?	1510 ± 5

nium are also given by Fig. 6. On the basis of the Engel theory,[5,6] any mixture of Re, Os, Ir, and Pt that had an average electron per atom concentration of 8 should show closely the same phase regions as indicated for osmium. A mixture with a concentration of 8.5 electrons per atom would show the phase regions indicated by a horizontal line half way between rhenium and osmium, and so forth. The structures corresponding to the various symbols of Figs. 6 and 7 are listed at the end of Table VII.

V) LITERATURE SURVEY OF SIMILAR SYSTEMS

The predicted[5] high stability of intermetallic binary compounds has now been verified for transition metals in addition to zirconium by the work of other researchers that will be summarized below and evaluated thermodynamically. Tables VIII to XI present some of the reactions observed. The Gibbs energies of the carbides given in Table V were used to evaluate the Gibbs energy limits of the intermetallic phases tabulated in Table XII.

A) The Stability of Niobium and Tantalum Compounds

Kaufman[60] studied reactions of NbC with Ru, Ir, and Pt; the results are summarized in Table VIII. As the lack of reaction at 1500 K with ruthenium could be due to either a very slow rate or unfavorable equilibrium, nothing can be said about the stability of Nb-Ru compounds. The formation of $NbIr_3$ and $NbPt_3$ fixes ΔF_f° < −32 kcal/mol at 1500 K based on ΔF_f° (NbC) given in Table V.

Table XI. Reactions of UC and UN with Ir, Rh, and Au,[61] and with Ru[68]

2 UC + Ir or Rh	→ U_2IrC_2 or U_2RhC_2	~1970 K
2 UC + Ru	→ U_2RuC_2	1570 K, 90 hr
UC + 3 Ir or 3 Rh	→ C + UIr_3 or URh_3	1670 K and 1970 K
UC + 3 Ru	→ URu_3C_x + (1-x)C	1570 K, 90 hr
UC + 3 Au(s)	→ UAu_3 + C	<1220 K, 17 hr 10^{-9} atm
UC + 3 Au(l)	→ UAu_3 + C	>1370 K, 118 hr 10^{-9} atm
UC_2 + 3 Au(s)	→ UAu_3 + 2C	1270 K
2 UN + 6 Au	→ $2UAu_3 + N_2$	1130 K, 47 hr 5×10^{-9} atm
UN + Au	→ U_2N_3 + Au	1130 K, 93 hr 0.75 atm N_2

Table XII. ΔF_f° Limits for Compounds of Nb, Ta, Hf, Th, Y, Ce, Er, U, and Pu from Reactions Reported in the Literature

Compound	ΔF_f° kcal/g-atom	Temperature	ΔF° was Obtained by Comparison with:
¼ $NbRe_{3\pm x}$ (χ)	> -8	2070 K	NbC
$TaRe_{1.5}$ (σ or χ)	$-3 > \Delta F_f^\circ > -8$	2730 K	TaC
$TaRe_{1.85}$ (χ)	$-3.5 > \Delta F_f^\circ > -7$	2700 K	TaC
$TaRe_{3.6}$ (χ)	-4.5 ± 1	2700 K	TaC
Hf_5Re_{24}	> -9	1800 K	HfC
URu_3	-11.4 ± 0.3	1000 K	EMF
¼ URu_3C_x	-15 ± 0.3	1000 K	EMF
U_2RuC_2	$-13 > \Delta F_f^\circ > -24$	1000 K	U_2C_3, URu_3C_x
$PuRu_2$	-6.6 ± 0.1	1000 K	EMF
$HfRh_3$	< −14	1800 K	HfB_2, HfC
$ThRh_2$	< −10 ?	2170 K	ThC_2
URh_3	< −7	1670-1970 K	UC_2
U_2RhC_2	< −10	~1970 K	UC
$NbIr_3$	< −8	1770 K	NbC
$HfIr_3$	< −14	2300 K	HfB_2, HfC
$ThIr_2$	< −10	~2000 K	ThC_2
YIr_2	< −11	1370-1770 K	YC_2
$CeIr_2$	< −11	1670 K	CeC_2
$ErIr_2$	< −11	1370-1670 K	ErC_2
UIr_3	< −7	1670-1970 K	UC_2
U_2IrC_2	< −10	~1970 K	UC
$NbPt_3$	< −8	1470-1770 K	NbC
$TaPt_3$	< −9	1670-1870 K	TaC
$HfPt_3$	-24 ± 4	2400 K	calorimetry
YPt	< −17	1370-1470 K	YC_2
CePt	< −17	1370 K	CeC_2
$CePt_2$	< −14	2170 K	CeS, Ce_3S_4
ErPt	< −17	1370-1670 K	ErC_2
UAu_3(s)	$-6.5 \geq \Delta F_f^\circ > -12.5$	1130-1370 K	UC, UN
UAu_3(ℓ)	−5	1725 K	vapor pressure

Several investigations[33-35] of the Nb-Re-C and Ta-Re-C ternary diagrams agree that rhenium and all Nb-Re and Ta-Re binary phases can coexist with NbC or TaC although as noted in the discussion of Section III-E of the Zr-Re-C results, an unknown θ phase with a diffraction pattern similar to that of rhenium is found with NbC or TaC. It is probably a ternary phase and may be metastable. Krikorian *et al.*[61] have defined the equilibria around 2700 K between the Ta-Re binary phases and TaC more quantitatively. They find $TaC_{0.7}$ in equilibrium with the rhenium-rich end (about 45 at. pct Re) of the bcc tantalum phase region and with $TaRe_{1.5}$ with the σ or χ structure depending upon the temperature. $TaC_{0.74}$ has a sufficiently lower tantalum activity to be in equilibrium with $TaRe_{1.85}$ with the χ structure.

$TaC_{0.92}$ is in equilibrium with the rhenium-rich end of the χ phase region with a composition around $TaRe_{3.6}$. To obtain Gibbs energies from these results, we must evaluate the thermodynamic activity of tantalum in $TaC_{0.7}$, $TaC_{0.74}$, and $TaC_{0.92}$ at 2700 K. Details of the calculations are given in Part B of the Appendix yielding $\Delta F_f^\circ = -21$ kcal/mol for $TaRe_{3.6}$ and $\Delta F_f^\circ > -10$ and > -8 kcal/mol for $TaRe_{1.85}$ and $TaRe_{1.5}$, respectively. These values are tabulated in Table XII as kcal/g-atom.

Raub and Falkenburg[62] observed reactions of both NbC and TaC with palladium and platinum at 1775 K to form graphite and fcc alloys; their data cannot be used for equilibrium calculations. Riesenfeldt[63] observed a reaction between TaC and platinum yielding $TaPt_3$ as given in Table VIII. After hot pressing for 0.5 h at both 1670 and 1870 K, an equimolar mixture was observed to contain carbon and the $TaPt_3$ phase indicating that the C-Ta-Pt ternary phase diagram is similar to the C-Zr-Ir diagram given in Fig. 1. The Gibbs energy limit in Table XII is based on the TaC value given in Table V.

B) The Stability of Hafnium and Thorium Compounds

Mercuri and Criscione[26] reported reactions of HfC and ThC_2 as well as ZrC with rhenium and iridium, Table IX. The authors proposed reactions with carbon as a product although no mention was made of observing it. Differential thermal analysis indicated that reaction commenced at around 1400 K. Heatings for 30 min at 1500 to 2470 K were used. The ThC_2 + Rh sample melted at 2170 K and the room temperature X-ray diffraction pattern could not be identified. The last reaction in Table VIII reported by Krikorian *et al.*[61] indicates that $ThAu_3$ is more stable than ThC, but the reaction was not well characterized and probably was a disproportionation of ThC to ThC_2.

Mercuri and Criscione[26] report HfB_2 and ZrB_2 react with rhenium and iridium as indicated in Table X. The starting materials were mixed powders. The reaction occurred by sintering in an induction furnace. Differential thermal analysis was used to detect the minimum temperature at which the reaction would support itself exothermally. The samples were then heated under vacuum for 0.5 h at 1700 K. X-ray analysis of the samples indicated that some boron had dissolved in the $HfRh_3$, $HfIr_3$, $ZrRh_3$, and $ZrIr_3$ phases; how much boron is not known because the lattice parameter (a_0) as a function of boron has not been determined.

With the excess of rhenium or iridium present, as given in Table X, the products might well be rhenium or iridium borides together with the AB_3 phase. The reaction might be approximated by

$$HfB_2 + 5Rh \rightarrow HfRh_3 + 2RhB$$

Reasonable estimates for the Gibbs energies of formation of RhB and IrB together with the value for HfB_2 yield the same limits for $HfRh_3$ and $HfIr_3$ as from the carbide reactions.

Fedorov *et al.*[31] studied the Hf-C-Re diagram. They had difficulty reaching equilibrium after 2130 h at 1770 K, but their diagram indicates HfC, C, and Re in equilibrium.

Ficalora[49] has burned $HfPt_3$ in a fluorine calorimeter to obtain $\Delta H_f^\circ = -132 \pm 9$ kcal/mol.

C) The Stability of Compounds of Lanthanides, Actinides and Other Group III Metals

Krikorian[64] reacted the dicarbides of Y, Ce, and Er with Ir and Pt, generally at 1370 K but with additional heatings up to 1770 K. YIr_2, $CeIr_2$, and $ErIr_2$ were produced. $CeIr_5$ was formed with excess iridium. YPt, CePt, and ErPt were produced with platinum. With excess platinum, the higher compounds, YPt_2, YPt_3, YPt_5, $CePt_2$, $CePt_5$, $ErPt_2$, $ErPt_3$, and $ErPt_5$ were produced. Krikorian assumed that for CeC_2 and ErC_2 $\Delta F_f^\circ = -33 \pm 2$ kcal/mol at 1500 K, the experimental[46] value for YC_2. For the various platinides and iridides formed, $\Delta F_f^\circ < -33$ kcal/mol at 1500 K.

Eastman *et al.*[65] found that CeS reacts with platinum according to $4CeS + 2Pt \rightarrow CePt_2 + Ce_3S_4$ at 2170 K. Evans[66] measured the heats of solution of CeS and Ce_3S_4 in 1 M HCl. Montgomery[67] measured the heat of solution of cerium metal as a function of HCl concentration from which one obtains -165.0 kcal/mol for the heat of solution of cerium metal in 1 M HCl and $\Delta H_{298}^\circ = 43$ kcal for $4CeS = Ce_3S_4 + Ce$. $(\Delta F_{2170}^\circ - \Delta H_{298}^\circ)/T$ was estimated to be -1 cal/K yielding $\Delta F_{2170}^\circ = 41$ kcal. Thus $\Delta F_f^\circ (CePt_2) < -41$ kcal/mol.

Krikorian *et al.*[61] studied reactions of cold pressed mixtures of UC and UN with Ir, Rh, and Au as listed in Table XI. Based on the reactions of Au with UC and UN, they fixed $\Delta F_f^\circ (UAu_3)$ between -25 and -50 kcal/mol. With two moles of UC plus 1 g-atom of iridium or rhenium, the ternary compounds U_2IrC_2 and U_2RhC_2 were formed. With excess metal, UIr_3 and URh_3 were formed. U_2IrC_2 melted at 2200 ± 20 K and UIr_3 melted at 2280 ± 20 K. Holleck and Kleykamp[68] have studied the corresponding reactions with ruthenium to obtain U_2RuC_2 for which they fix ΔF_f° at 1000 K between -63 and -120 kcal/mol. With excess ruthenium, they observe the reaction $UC + 3Ru = URu_3C_x + (1 + x)C$. URu_3C_x and URu_3 have the cubic Cu_3Au type structure and they form a continuous solid solution. High temperature galvanic cells with solid CaF_2 electrolyte were used to fix ΔF_f° at 1000 K as -45.5 ± 1 kcal/mol for URu_3 and -60.1 ± 1 kcal/mol for URu_3C_x. Campbell *et al.*[69] have used similar galvanic measurements for $PuRu_2$ to obtain $\Delta F_f^\circ = -19.9$ kcal/mol at 1000 K. Holleck and Kleykamp[68] have also used equilibria between $(U_{0.8}Pu_{0.2})O_{2-x}$ and $(U_{0.8}Pu_{0.2})Me_3$, where Me corresponds to a mixture of Ru, Rh, and Pd, to fix ΔF_f° of $(U_{0.8}Pu_{0.2})Me_3$ at 2000 K as less than -45 kcal/mol. Alcock and Grieveson[75] have measured vapor pressures of gold over Au-U liquids between 1725 and 1825 K between 17 and 90 at. pct Au. For UAu_3(liq) at 1725 K, their results give $\Delta F_f^\circ = -20$ kcal/mol. These data are summarized in Table XII in kcal/g-atom.

D) The Stability of Additional Platinum Compounds

Bronger and Klemm[70] made several platinum compounds: Pt_3Al, $Pt_{13}Al_3$, Pt_3Sc, Pt_5Y, Pt_4La, $Pt_{15}Be$, Pt_3Mg, Pt_7Mg, Pt_2Ca, Pt_7Ca_2, Pt_5Ca, Pt_2Sr, Pt_3Sr, Pt_5Sr, Pt_7Li, and Pt_3Cr. The nonprecious metal oxides (Al_2O_3, Sc_2O_3, and so forth) were reduced in the presence of platinum and H_2. The crystal structures and lattice constants of the compounds are discussed. To estimate the Gibbs energies of formation from the reactions described in the article, information additional to that given in the article must be known or assumed. Corre-

spondence with Dr. Bronger has provided the information needed to set limits on the Gibbs energies of formation of many of these compounds. These values will be published.[78] Similar observations for oxides of Zr, Hf, Th, Pa, U, Np, and Pu with Pt group metals have been reported by Erdman and Keller.[93]

E) Tabulation of Gibbs Energies

Table XII lists the limits of the standard state Gibbs energies of formation in kcal/g-atom of alloy of the various compounds reviewed that are based on the observed reactions with the carbides, the borides, and the nitrides listed in Tables VIII to XI. The question marks indicate the values for which authors have expressed some uncertainty. The temperature for which ΔF_f° was calculated is given. As ΔS_f° is small, the values can be used over a range of several hundred Kelvin. Limits on the standard state Gibbs energies of formation of other compounds of a particular binary system can be expressed as they were in Table VII; the necessary steps are outlined in Appendix A.

VI) DISCUSSION

Although the ΔF values of Tables VI, VII, and XII and Fig. 5 are mostly upper or lower limits rather than narrowly defined values, they are quite sufficient to confirm the prediction that extraordinarily stable intermetallic compounds will result when transition metals with low-lying empty $4d$ or $5d$ orbitals are combined with transition metals with six or more $4d$ or $5d$ electrons per atom. The dotted lines of Fig. 5 indicate the expected values on the basis of the relative bonding energies of $4d$ and $5d$ electrons.[6] As Fig. 5 illustrates, compounds of rhenium have the characteristically low stabilities usually associated with intermetallic compounds. There is a pronounced increase in stability when rhenium is replaced by ruthenium metal, which has the electronic configuration d^6sp. The stability increases with additional electrons reaching a maximum in the group Rh, Ir, Pd, and Pt and then drops off with silver and gold. Size and internal-pressure differences[5] play a role in determining these trends, but the overwhelming factor is the more complete utilization in the bonding of the electrons of the transition metal from the right hand side of the periodic table through exploitation of the vacant d and p orbitals of the metal from the left hand side. Table XII presents data for additional transition metal systems. Insufficient data are available for metals other than zirconium to verify some of the predictions of the Engel model in regard to the position of the maximum in stability. However, the ability of even the 50 at. pct MPt phases of Y, Ce, and Er to coexist with carbon, whereas the activities of Zr, Hf, Nb, and Ta are not sufficiently reduced to coexist with carbon until the platinum content is increased to 75 at. pct, would tend to verify the prediction that the position of maximum stability would shift from iridium to platinum as the left hand metal is varied from Nb to Zr to Y. It is hoped that sufficient data will become available soon to check these predictions quantitatively and to narrow down the regions of greatest stability.

It is clear that such unusual intermetallic compounds, which compare in stability with the most stable of compounds of metals together with nonmetals, warrant additional attention. They can be expected to have some unique properties. A few of the properties have been measured in this study. They are very high melting, mostly in the range above 2000 K. They are metallic conductors but not superconductors with high transition temperatures. They are very inert to chemical attack by etching solutions or by oxygen even at very high temperatures, but they can be attacked by fluorine. They tend to be very hard and brittle. Because of their high thermodynamic stability, they can be readily formed by a variety of high temperature reactions. For example, it would be easy to prepare thin coatings of these hard inert materials by vapor deposition or electroplating. Caution is advised in preparing large batches of these compounds directly from the elements as an explosion has been reported[6] upon heating hafnium and platinum together due to the very large heat evolution. As $HfPt_3$ has an enthalpy of formation of -135 kcal/mol and one can assume an average heat capacity of 7 cal/g-atom or 38 cal/mol, the initiation of reaction of a mixture of Hf + 3Pt at 1000 K would cause a temperature jump of almost 5000 K under adiabatic conditions. If the hafnium should contain much hydrogen, as is commonly the case, the violence of the explosion is enhanced.

There are interesting chemical applications of the expected high stability of the platinum group compounds of the lanthanides and actinides. In a fused salt containing a variety of lanthanides and actinides, it should be possible to preferentially extract certain of these elements into precious metal foils by control of the alloy content of the foil and the oxidizing-reducing potential of the fused salt. Likewise precious metal foils could be used as gettering agents to extract lanthanide or actinide metals from the gaseous phase.

The theoretical implications of the demonstration of these very stable intermetallic compounds are a challenge to theories of bonding. They verify the important distinct role played by d electrons in contrast to the s and p electrons as emphasized by the Engel theory of metals. Most theories that have been commonly applied to metals have not provided even the slightest indication that such drastically different behavior should be anticipated. Certainly with respect to reactivity with transition metals from the left hand side of the periodic tables, the platinum group metals are not to be classed as noble metals.

APPENDIX

CALCULATION OF THERMODYNAMIC DATA FROM TERNARY PHASE DIAGRAMS

The calculation of thermodynamic data from the respective ternary phase diagrams has been briefly outlined in Section IV. A more complete description follows.

A) Calculation of Activity Coefficients from Ternary Phase Diagrams

To illustrate how activity coefficients are obtained from the ternary phase diagram presented, the C-Zr-Ru phase diagram will be used as an example. The derived activities (a_i) and activity coefficients (γ_i) are based upon the solvent standard state, *i.e.*, when $X_i = 1$ (X_i = the mole fraction of component i), $a_i = 1$ and $\gamma_i = 1$.

When the C, ZrC, and Ru phases exist in equilibrium, the activities of all the components in the three phases are fixed. The activity of ruthenium (a_{Ru}) is close to one since very little zirconium (0.75 at. pct Zr) and presumably a negligible amount of graphite dissolved into the ruthenium phase. The activity of graphite (a_C) is equal to one because of the presence of pure graphite. Since all of the phases are in equilibrium with each other, the activity of each component is the same in all three phases:

$$a_{Ru}^{Ru} = a_{Ru}^{C} = a_{Ru}^{ZrC} = 1$$

$$a_{C}^{C} = a_{C}^{ZrC} = a_{C}^{Ru} = 1$$

$$a_{Zr}^{ZrC} = a_{Zr}^{Ru} = a_{Zr}^{C} = \text{constant}$$

The superscripts designate the phase being discussed; for example, a_{Ru}^{ZrC} represents the activity of ruthenium in the ZrC phase. The activity of zirconium can be calculated because the ΔF_f° (ZrC) is known; at 1770 K, ΔF_f° (ZrC) = −44.2 kcal/mol. ΔF_f° (ZrC) may also be expressed as:

$$\Delta F_f^\circ (ZrC) = +RT \ln a_C a_{Zr}$$

Using the appropriate values:

$$-44.2 \text{ kcal/mol} = R(1770) \ln [(1)(a_{Zr})]$$

$$\log a_{Zr} = \frac{-44.2 \times 10^3}{(2.303)(1.987)(1770)} = -5.46$$

$$a_{Zr} = 10^{-5.46}$$

As stated above, the a_{Zr} is the same in all phases. For the ruthenium phase:

$$a_{Zr}^{Ru} = \gamma_{Zr}^{Ru} X_{Zr}^{Ru} = 10^{-5.46}$$

From the microprobe analysis of the C-Zr-Ru samples:

$$X_{Zr}^{Ru} = 0.0075 = 10^{-2.125}$$

Therefore:

$$\gamma_{Zr}^{Ru} = a_{Zr}^{Ru} / X_{Zr}^{Ru} = 10^{-5.46}/10^{-2.125}$$

$$\gamma_{Zr}^{Ru}(0.75 \text{ at. pct Zr}) = 10^{-3.335}$$

This result will be used in Part B to calculate ΔF_f° ($ZrRu_2$).

It is useful to know the activity coefficient of an element at the limit of 0 pct of that element in an alloy for comparison of γ values in different metal solvents under conditions where solute-solute interactions play no role. In many systems, the relation $\log \gamma_2 = wX_1^2$, where X_1 is the mole fraction of the other component and w is a function of temperature, is found to hold approximately[14] and this equation was used for short extrapolations to $X_2 = 0$ or $X_1 = 1$. For example, $\log \gamma_{Zr}^{Ru}(X_{Zr} \rightarrow 0)$ $= -3.335/(0.9925)^2 = -3.39$, the value tabulated in Table VI.

The C-Zr-Re, C-Zr-Os, C-Zr-Ag, and C-Zr-Au ternary phase diagrams are similar to the C-Zr-Ru phase diagram as indicated in Fig. 4. Because only limits could be placed on the composition of the zirconium binary alloys of Re, Os, and Ag in equilibrium with carbon and ZrC, only limits can be placed on γ_{Zr} and the small extrapolation to infinite dilution is negligible. The method of calculating γ_{Zr} will be illustrated for rhenium. Gorshkova *et al.*[35] report that a mixture of 0.99 g-atom Re with 0.005 moles ZrC showed the presence of ZrC after 200 h at 2170 K. As the system may not be at unity activity of carbon, one may only fix a_{Zr} as $\geq 10^{-4.3}$ from the ΔF values in Table V for ZrC and γ_{Zr} as $>10^{-1.6}$. $\Delta \bar{F}_{Zr}^{xs} > -16$ kcal/g-atom at 2170 K. Within the uncertainties of the limits, the same limits can be used at 1800 K as in Table VI. The osmium values were obtained in a similar manner. The silver and gold calculations are discussed in detail in Part B of the Appendix.

To determine γ_{Zr} (0 pct Zr) in Ir, Rh, Pt, and Pd is more difficult as a longer extrapolation must be made. For each of these systems, the ZrM_3 phase was found to be in equilibrium with carbon and ZrC. For iridium and rhodium, this was confirmed[26] between 1475 and 2475 K. Only a small temperature coefficient is expected and the same equilibrium is expected at all temperatures up to the liquidus. Since the measurements for palladium and platinum extended from 1650 to 1850 K, the calculations will be carried out for a temperature of 1800 K for all four metals. From the ΔF° (ZrC) from Table V, $a_{Zr} = 10^{-5.35}$ for ZrC + C at 1800 K. For ZrM_3, $X_{Zr} = 0.25 = 10^{-0.602}$ and $\gamma_{Zr} = 10^{-4.7}$.

The extrapolation to 0 pct Zr will be illustrated for the Zr-Pt system for which ΔH_f° ($ZrPt_3$) = −123.5 ± 6 kcal/mole is known.[49] $\Delta C_p^\circ = -2$ cal/deg mole and $\Delta S_f^\circ = -4$ cal/deg mole are reasonable estimates up to 1100 K yielding ΔF_f° ($ZrPt_3$) = −121 ± 8 kcal/mole at 1100 K. Extrapolation to 1800 K would yield ΔF_f° ($ZrPt_3$) = −119 ± 9 kcal/mole and $a_{Zr}\, a_{Pt}^3 = 10^{-14.5 \pm 1}$. For carbon saturated $ZrPt_3$, $a_{Zr} = 10^{-3.1 \pm 0.4}$ and $\gamma_{Pt} = 10^{-2.9}$. These values are for some composition within the $ZrPt_3$ homogeneous range and we must extrapolate to the platinum-rich composition in equilibrium with the cubic platinum phase. To proceed we need information about the phase diagram between $ZrPt_3$ and platinum. It has been predicted[5] that the fcc phase of platinum would extend, at high temperatures, to $ZrPt_{3.5}$ with only a narrow two phase region between the hexagonal and cubic phase regions. This prediction has been recently confirmed.[88] The two values[49,88] of 18 at. pct Zr at 1173 K and 20 at. pct Zr at 1923 K for the composition of the cubic phase saturated by $ZrPt_3$ yields 1500 cal for the enthalpy of solution of $ZrPt_3$ in the cubic solid solution. Also Worrell and Meschter[48] have determined from electromotive force measurements that $(41/14)\Delta H_f(ZrPt_3) - (27/14)\Delta H_f$ ($ZrPt_{41/9}$) = −102 kcal in the range 1073 to 1273 K. Also, Worrell and Meschter have found $\log a_{Zr} = -17.5$ for coexisting $ZrPt_3$ and $ZrPt_{41/9}$ at 1100 K. From the value of ΔF_f° ($ZrPt_3$) at 1100 K given above, one calculates $\log a_{Pt}$ $= -1.9 \pm 0.5$. These values yield ΔF_f° ($ZrPt_{41/9}$) = −135 ± 11 kcal/mole and ΔH_f° ($ZrPt_{41/9}$) = −136 ± 12 kcal/mole at 1100 K. $\Delta \bar{H}_{Pt} = -8 \pm 4$ kcal/g-atom is obtained for the $ZrPt_{41/9}$ solution. Extrapolation of these results to 1800 K yield $\log a_{Pt} = -1.5 \pm 0.6$ and $\log a_{Zr} = -9.3 \pm 2$ for the $ZrPt_3$-$ZrPt_{3.5}$ mixture at 1800 K. For $ZrPt_{3.5}$, $\log \gamma_{Zr} = -9.0 \pm 2$ and $\log \gamma_{Pt} = -1.4$ Extrapolation across the fcc solid solution is more difficult. The activity coefficient of platinum increases from 0.04 to 1 as X_{Pt} increases from 0.78 to 1. The manner in which the platinum activity coefficient increases determines the change in γ_{Zr} as required by the Gibbs-Duhem equation[14]

$$d \log \gamma_{Zr} = -(X_{Pt}/X_{Zr})\, d \log \gamma_{Pt}$$

Between $X_{Pt}/X_{Zr} = 3.5$ and infinity, $\log \gamma_{Pt}$ changes by 1.4. It can be immediately seen that the smallest change in γ_{Zr} takes place if the change in γ_{Pt} takes place before

X_{Pt}/X_{Zr} has increased appreciably and the minimum change in $\log \gamma_{Zr}$ is $-3.5(1.4) = -4.9$ yielding $\log \gamma_{Zr}$ (0 pct Zr) $\leq -13.9 \pm 2$. Thus the upper limit of $\log \gamma_{Zr}$ (0 pct Zr) is -11.9. Various solution models can be assumed such as ideal mixing of $ZrPt_3$ and platinum or mixing with a positive deviation almost sufficient for phase separation, and so forth, and various limiting $\log \gamma_{Zr}$ (0 pct Zr) values less than -12 can be calculated corresponding to $\Delta \bar{F}^{xs}_{Zr}$ values around -100 kcal/g-atom Zr in very dilute solutions of zirconium in platinum. At 1800 K, $\Delta F^\circ_f(ZrO_2) = -182$ kcal/mol and $a_{Zr} P_{O_2} = 10^{-22}$. With $\gamma_{Zr} < 10^{-12}$, one calculates that platinum in equilibrium with ZrO_2 and an oxygen pressure of 10^{-7} atm would dissolve more than 0.1 at. pct Zr. Under reducing conditions, the concentration of zirconium would be much higher. Thus the reason for the reaction between platinum thermocouple wires and ZrO_2 protection tubes under reducing conditions becomes clear.

For Ir, Rh, and Pd, we only have an upper limit to ΔF°_f of the ZrM_3 compounds. The extrapolation of $\gamma_{Zr} = 10^{-4.7}$ for $X_{Zr} = 0.25$ to γ_{Zr} (0 pct Zr) $< 10^{-7}$ given in Table VI was made by making the very conservative estimate that γ_{Zr} (carbon saturated ZrX_3)/γ_{Zr} ($X_{Zr} = 0$) is greater than $10^{2.3}$ in Ir, Rh, and Pd compared to the value of $10^{7.3}$ in platinum.

B) The Gibbs Energy of Formation of Binary Phases from Ternary Phase Diagrams

From ternary phase diagrams such as those of Figs. 1 and 4, limits can be placed on the Gibbs energies of formation (ΔF°_f) of all the intermetallic binary zirconium compounds represented in the ternary diagrams.

Considering the C-Zr-Ir system first, the following reaction may be written because ZrC and iridium cannot exist in equilibrium according to the ternary phase diagram presented in Fig. 1.

$$ZrC + 3Ir \rightarrow ZrIr_3 + C$$

This reaction was actually observed at 1770 K, as discussed in Section III-A; thus,

$$\Delta F^\circ_{rx} = \Delta F^\circ_f(ZrIr_3) - \Delta F^\circ_f(ZrC) \leq 0$$

From Table V, $\Delta F^\circ_f(ZrC) = -44.2$ kcal/mol at 1800 K and $\Delta F^\circ_f(ZrIr_3) \leq \Delta F^\circ_f(ZrC) = -44.2$ kcal/mol at 1800 K. The limit on $\Delta F^\circ_f(ZrIr_3)$ ~ -11 kcal/g-atom is therefore obtained.

With a knowledge of what Zr-Ir compounds are thermodynamically stable with respect to each other, more limits may be determined. The following inequality is true for such compounds in the Zr-Ir system:

$$\tfrac{1}{3}\Delta F^\circ_f(Zr_3Ir) \geq \tfrac{1}{2}\Delta F^\circ_f(Zr_2Ir) \geq \tfrac{3}{5}\Delta F^\circ_f(Zr_{5/3}Ir) \geq \Delta F^\circ_f(ZrIr) \geq \Delta F^\circ_f(ZrIr_2) \geq \Delta F^\circ_f(ZrIr_3) \quad [1]$$

The above can be rationalized by considering reactions such as:

$$ZrIr_2 + Ir \rightarrow ZrIr_3$$

and

$$\tfrac{1}{3}Zr_3Ir + \tfrac{1}{6}Ir \rightarrow \tfrac{1}{2}Zr_2Ir$$

$\Delta F^\circ_{rx} \leq 0$ for both reactions because these Zr-Ir compounds are reported to be stable with respect to each other. Another similar inequality is true:

$$\Delta F^\circ_f(Zr_3Ir) \leq \Delta F^\circ_f(Zr_2Ir) \leq \Delta F^\circ_f(Zr_{5/3}Ir) \leq \Delta F^\circ_f(ZrIr) \leq \tfrac{1}{2}\Delta F^\circ_f(ZrIr_2) \leq \tfrac{1}{3}\Delta F^\circ_f(ZrIr_3) \quad [2]$$

which can be rationalized by considering reactions such as:

$$Zr_2Ir + Zr \rightarrow Zr_3Ir$$

and

$$\tfrac{1}{3}ZrIr_3 + \tfrac{1}{6}Zr \rightarrow \tfrac{1}{2}ZrIr_2$$

where $\Delta F^\circ_{rx} \leq 0$. The ΔF°_f's expressed in Inequalities [1] and [2] have units of kcal/mol; the ΔF°_f's in Table VII are expressed in kcal/g-atom. These same inequalities can be derived by considering free energy diagrams as presented by Darken and Gurry.[89] Using Inequality [2] along with the inequality $\Delta F^\circ_f(ZrIr_3) \leq -44.2$ kcal/mol, the limits of Table VII can be obtained. Inequality [1] would be used if there were any compounds to the iridium-rich side of $ZrIr_3$.

The ternary systems represented in Fig. 4 are different. For ruthenium alloys it has experimentally been determined at 1770 K that ruthenium (0.75 at. pct Zr) exists in equilibrium with the carbon and the ZrC phases and that the $ZrRu_2$ and the ruthenium (1.15 at. pct Zr) binary phases exist in equilibrium without the presence of both carbon and ZrC. The experimental details used to obtain these conclusions have been covered in Sections III-C and III-D. From this information the $\Delta F^\circ_f(ZrRu_2)$ can be calculated and additional phase diagram data used to fix the Gibbs energy of ZrRu, the only other known Zr-Ru intermediate phase.

From the three phase equilibrium of C, ZrC, and Ru (0.75 at. pct Zr) at 1770 K, $a_{Zr} = 10^{-5.46}$ and γ_{Zr} (0.75 at. pct Zr) $= 10^{-3.335}$ as calculated previously. In Part A of this Appendix, it was assumed that $\log \gamma_{Zr}$ was proportional to the square of the mole fraction of ruthenium to extrapolate to 0 pct Zr. The same assumption can be made to extrapolate from 0.75 at. pct to 1.15 at. pct Zr.

$$\log \gamma_{Zr} \text{ (1.15 at. pct Zr)} = -3.335(0.9885/0.9925)^2 = -3.31$$

and

$$\log a_{Zr} = -3.31 - 1.94 = -5.25$$

For such a dilute solution, the activity of ruthenium can be approximated by its mole fraction, a_{Ru} (1.15 at. pct Zr) = 0.9985. As ruthenium (1.15 at. pct Zr) is in equilibrium with $ZrRu_2$ at 1770 K, the activities of zirconium and ruthenium must be the same for the two phases. Since $\Delta F^\circ_f(ZrRu_2) = 2.303RT \log_{10}(a_{Zr})(a_{Ru})^2$, $\Delta F^\circ_f(ZrRu_2) = 4.576(1770)(-5.25 - 2 \times 0.005) = -42.5$ kcal/mol or -14.2 kcal/g-atom at 1770 K. This value is based on the various experimentally determined concentrations of zirconium. From the microprobe analysis of a $Zr_{0.6}Ru_{99.4}$ test standard, the zirconium concentrations are in error by less than ±37 pct of the amount present; the corresponding error associated with the calculated $\Delta F^\circ_f(ZrRu_2)$ is ±2.7 kcal/mol or ±0.9 kcal/g-atom. In the calculations it was assumed that $\log \gamma_{Zr}$ varies as $(X_{Ru})^2$ between 0.75 and 1.15 at. pct Zr and that $\gamma_{Ru} = 1$ from 0 to 1.15 at. pct Zr.

Raub and Rõschel[71] report that $ZrRu_2$ decomposes below 1570 K to ZrRu and ruthenium. At 1570 K, $\Delta F_f(ZrRu_2) = \Delta F_f(ZrRu)$. Extrapolation of the $ZrRu_2$ value

from 1770 K yields ΔF_f(ZrRu) = −43 ± 3 kcal/mol at 1570 K.

A similar procedure can be followed for the Zr-Au alloys. The calculation is more involved because the equilibration of C, ZrC, and Au (9.5 at. pct Zr) was done above the melting points of gold and $ZrAu_4$ and the ΔF_f°'s are desired for solid alloys.

It has been experimentally determined that graphite and ZrC are in equilibrium with gold (liquid, 9.5 ± 3.5 at. pct Zr) at 1770 K and that $ZrAu_4$ is in equilibrium[17] with gold (solid, 7.3 at. pct Zr) and gold (liquid, 5.9 at. pct Zr) at 1340 K. From ΔF_f°(ZrC) we calculated $a_{Zr} = 10^{-5.46}$ and $\gamma_{Zr} = 10^{-4.44}$ at 1770 K. The assumption that $\log \gamma_{Zr}$ varies as the square of the mole fraction of gold yields $\log \gamma_{Zr}$ (5.9 at. pct Zr, 1770 K) = −4.44 × $(0.941/0.905)^2$ = −4.8 and $\Delta \bar{F}_{Zr}^{xs} = 2.303R(1770)(-4.8)$ = −39 kcal/mol at 1770 K. The assumption of an excess partial molal entropy of −3 cal/K mol yields $\Delta \bar{F}_{Zr}^{xs}$ = −40 kcal/mol at 1340 K or γ_{Zr} (5.9 at. pct Zr) = $10^{-6.5}$. Thus $a_{Zr} = 10^{-7.7}$ for gold (liquid, 5.9 at. pct Zr), gold (solid, 7.3 at. pct Zr), and $ZrAu_4$ at 1340 K. For gold (solid, 7.3 at. pct Zr), $\log \gamma_{Zr}$ = −6.6 and the value of $\log \gamma_{Zr}$ (0 at. pct Zr) = $-6.6/(0.927)^2$ = −7.7 at 1340 K. To calculate ΔF_f° of $ZrAu_4$, we must obtain the activity of gold in either the 5.9 at. pct Zr liquid or the 7.3 at. pct Zr solid. Estimates range from 0.84 to 0.88. ΔF_f° ($ZrAu_4$) = $2.303R(1340)[-7.7 - 4(0.06)]$ = −49 kcal/mol at 1340 K. If one considers the uncertainties of the determination of the concentration of zirconium in equilibrium with ZrC and graphite, the resulting uncertainty in $\log \gamma_{Zr}$ is represented by $\log \gamma_{Zr}$ (liquid, 5.9 at. pct Zr, 1340 K) = −7.7 ± 0.03 and the uncertainty in the Gibbs energies is ±2 kcal/mol Zr. If $ZrAu_4$ disproportionates at around 1400 K to $ZrAu_3$ plus a liquid with about 8 at. pct Zr ($a_{Au} \sim 0.8$) as indicated by Shunk,[17] then $\Delta F_f^\circ(ZrAu_3)$ = −48 kcal/mol at 1400 K. Limits of the ΔF_f° of other Zr-Au alloys given in Table VII follow directly from Inequalities [1] and [2].

Although the C-Zr-Re, C-Zr-Os, and C-Zr-Ag phase diagrams are also of the type represented in Fig. 4, the method of estimating ΔF_f° of these compounds represents still another case. Since carbon reacts with all binary compounds of Zr with Re, Os, and Ag to form ZrC, all of these compounds must have ΔF_f° values more positive than that of ZrC. The limits given in Table VII for Zr-Re phases were obtained in this manner. For osmium and silver, closer limits can be placed. From Table III, the osmium phase in equilibrium with ZrC + C at 1800 K contains less than 0.059 at. pct Zr. The value of $\gamma_{Zr} \geq 10^{-2.1}$ from Table VI was calculated from ΔF_f°(ZrC). The maximum solubility of zirconium in osmium has been estimated[5] at 15 at. pct. At 1800 K, the solubility should be reduced to about 10 at. pct. The assumption of $\log \gamma_{Zr} = wX_{Os}^2$ yields $\log \gamma_{Zr}$ > −1.7 and $\log a_{Zr}$ > −2.7 at X_{Os} = 0.9. A reasonable limit to a_{Os} at X = 0.9 is >0.84. $\Delta F_f^\circ(ZrOs_2) > 2.303R$ × (1800)(−2.7 − 0.14) = −23 kcal/mol. The limits for the other Zr-Os phases were obtained from Inequality [1].

It is possible to obtain a closer limit for the ΔF_f° of the silver compounds by using the phase diagram[15,86] that indicates that ZrAg is in equilibrium with silver liquid containing 2.9 at. pct Zr at 1228 K. The data of Table IV indicate the ZrC + C are in equilibrium with silver liquid containing less than 0.05 at. pct Zr at 1680 K. From the ΔF_f° value of ZrC in Table V, $\Delta \bar{F}_{Zr}^{xs}$ = −44.6 kcal/mol in this solution. The assumption of $\Delta \bar{S}^{xs}$ = 4 cal/K mol for Zr(s) = Zr(Ag liquid solution) yields $\Delta \bar{F}^{xs}$ > −42.8 kcal/mol for a silver liquid solution at 1228 K containing 0.05 at. pct Zr. This corresponds to $a_{Zr} > 10^{-7.6}$ and $\gamma_{Zr} > 10^{-4.3}$. The assumption that $\log \gamma_{Zr}$ varies as the square of the silver mole fraction yields $\gamma_{Zr} > 10^{-4.05}$ and $a_{Zr} > 10^{-5.6}$ for a silver liquid solution with 2.9 at. pct Zr. The silver activity is close to unity, so ΔF_f°(ZrAg) > 2.303R(1228)(−5.6) = −31 kcal/mol at 1228 K. Through use of Inequality [1], $\Delta F_f^\circ(\frac{1}{2}ZrAg) > -31$ kcal/mol. Pravoverov and Kolonin[90] have reported the solubility of ZrAg in silver solid at 1176 K to be 0.17 at. pct Zr from which one can calculate $\log \gamma_{Zr} > -3.1$ in solid silver at 1175 K.

The equilibria between Ta-Os phases and the TaC_x phase were reviewed in Section VI-A. Their evaluation requires values of $\Delta F_f^\circ(TaC_x)$ at 2700 K as a function of x. Extrapolation of the values for $TaC_{0.5}$ and TaC in Table V to 2700 K yield −22.0 and −35.3 kcal/mol, respectively. The Gibbs energy functions tabulated by Storms[39] for $NbC_{0.5}$, $NbC_{0.75}$, and $NbC_{0.97}$ serve as guides for the estimation of corresponding values for the tantalum carbide phases including some contribution for randomization. These Gibbs energy functions together with the equation[39] for variation of the enthalpy of formation of TaC_x as a function of x yield ΔF_f° = −27.5 ± 2, −28 ± 2, and −33.5 ± 2 kcal/mol, respectively, for $TaC_{0.70}$, $TaC_{0.74}$, and $TaC_{0.92}$. ΔF_{2100}° = 35.3 kcal for TaC = Ta + C yields $a_{Ta} = 10^{-2.9}$ for carbon saturated TaC. ΔF° = 8 kcal for $3.5TaC_{0.5} = 2.5TaC_{0.7}$ + Ta and ΔF° = 28 kcal for $5Ta_{0.7} = 5TaC_{0.5}$ + C yield $a_{Ta} = 10^{-0.6}$ and $a_C = 10^{-2.3}$ for the metal-rich end of the TaC phase region at 2700 K. Hoch *et al.*[91] report a_C for TaC_x as a function of x; their results have been modified to fit the boundary values. For $TaC_{0.70}$ at 2700 K, $a_{Ta} = 10^{-0.6}$ and $a_C = 10^{-2.3}$. For $TaC_{0.74}$, $a_{Ta} = 10^{-0.8}$ and $a_C = 10^{-1.9}$. For $TaC_{0.92}$, $a_{Ta} = 10^{-1.7}$ and $a_C = 10^{-1.1}$. These values of a_{Ta} yield ΔF_f° = −21, −10, and −8 kcal/mol for $TaRe_{3.6}$, $TaRe_{1.85}$, and $TaRe_{1.5}$ respectively, assuming unit activity of rhenium. The activity of rhenium should be close to unity for $TaRe_{3.6}$, but the ΔF_f° values for the other two phases must be upper limits. Inequality [1] sets lower limits. These values are tabulated in Table XII as kcal/g-atom.

ACKNOWLEDGMENTS

The assistance offered by the staff of the Inorganic Materials Research Division of the Lawrence Berkeley Laboratory and the financial support provided by the Atomic Energy Commission is gratefully acknowledged.

REFERENCES

1. L. Pauling: *Proc. Roy. Soc. London,* Ser. A, 1949, vol. 196, pp. 343-62 and *The Nature of the Chemical Bond,* 3rd ed., Cornell U. Press, Ithaca, New York, 1960.
2. C. A. Coulson: *Valence,* 2nd ed., Oxford Univ. Press, Oxford, 1963.
3. J. W. Linnett: *Wave Mechanics and Valency,* Methuen, London, 1966.
4. N. Engel: *Some New Viewpoints on the Metallic Bond,* Ingenioeren M101 (1939), M1 (1940); Haandogi Metallare, Selskabet for Metalforskning, Copenhagen, 1945; *Kem. Maandesb.,* 1949, vol. 30, no. 5, p. 53; no. 6, p. 75; no. 8, p. 97; no. 9, p. 105; no. 10, p. 114; *Powder Met. Bull.,* 1954, vol. 7, pp. 8-18; *Amer. Soc. Metals, Trans.,* 1964, vol. 57, 610-19; and *Acta Met.,* 1967, vol. 15, 557-63.
5. L. Brewer: in *Electronic Structure and Alloy Chemistry of the Transition Elements,* P. A. Beck, ed., pp. 221-35, Interscience, New York, 1963; Dover, N. Y., 1965, and *High-Strength Materials,* V. F. Zackay, ed., chap. 2,

pp. 12-103, John Wiley and Sons, N. Y., 1965. (An earlier draft was distributed as UCRL-10701, 1963.)
6. L. Brewer: *Phase Stability in Metals and Alloys,* P. Rudman, J. Stringer, R. I. Jaffee, eds., pp. 39-61, 241-49, 344-46, and 560-68, McGraw-Hill, N. Y., 1967; *Acta Met.,* 1967, vol. 15, 553-56; and Science, 1968, vol. 161, 115-22.
7. W. Hume-Rothery: *Acta Met.,* 1965, vol. 13, 1039-42 and *Progress in Materials Science,* 1968, vol. 13, no. 5, pp. 229-65.
8. L. Brewer: *Plutonium 1970 and Other Actinides,* W. N. Miner, ed., pp. 650-58, *TMS Nucl. Met. Ser.* Vol. 17, Metallurgical Soc. AIME, N. Y., 1970.
9. L. Brewer: *J. Opt. Soc. Amer.,* 1971, vol. 61, pp. 1101-11 and 1666-82.
10. Paul R. Wengert: Ph. D. Thesis, University of California, Berkeley, UCRL-18727, April 1969, 118 pp., on which the present paper is largely based. Available from University Microfilms, Ann Arbor, Michigan; order No. 70-6258.
11. Larry D. Hartsough: Ph. D. Thesis, University of California, Berkeley, September 1971, LBL-119.
12. Barton William Olinger: June 1970, Ph. D. Thesis, University of Chicago, June 1970.
13. C. E. Moore: *Atomic Energy Levels,* Nat. Bur. Stand. U. S. Circ. 467, U. S. Govt. Printing Office, Washington, D. C., vols. 1-3, 1949, 1952, 1958.
14. G. N. Lewis and M. Randall: *Thermodynamics,* 2nd ed., revised by K. S. Pitzer and L. Brewer, Chap. 6, 21, and 32, McGraw-Hill Book Co., New York, 1961.
15. M. Hansen: *Constitution of Binary Alloys,* McGraw-Hill Book Co., New York, 1958.
16. R. P. Elliott: *Constitution of Binary Alloys,* First Supplement, Mc-Graw Hill Book Co., New York, 1965.
17. F. A. Shunk: *Constitution of Binary Alloys,* Second Supplement, McGraw-Hill Book Co., New York, N. Y., 1969.
18. The multistation hot press was designed by and built under the supervision of Milton R. Pickus for use in the Inorganic Materials Research Division of the Lawrence Berkeley Laboratory, University of California, Berkeley, California 94720.
19. J. Z. Frazer, R. W. Fitzgerald, and A. M. Reid: Computer Programs EMX and EMX2 for Electron Microprobe Data Processing, from Electron Probe Analysis Society of America, Proceedings of the First National Conference, 1966. Available from L. F. Vassamillet, Carnegie-Mellon Institute, Pittsburgh, Pa. 15213.
20. L. S. Birks: *Electron Probe Microanalysis,* p. 125, Interscience Publishers, New York, 1963.
21. H. A. Elion: *Instrumental and Chemical Analysis Aspects of Electron Microanalysis and Macroanalysis,* vol. 5 of *Analytical Chemistry,* Series IX of *Progress in Nuclear Energy,* Pergamon Press, London, 1966.
22. J. W. Colby: *Adv. in X-ray Analy.,* vol. 11, Plenum Press, 1968.
23. R. D. Giauque: *Analy. Chem.,* 1968, vol. 40, pp. 2075-77.
24. H. S. de Ben: Estimation of Detection Limits in Electron Probe Microanalysis, from Electron Probe Analysis Society of America, Proceedings of the Third National Conference, 1968. Available from L. F. Vassamillet, Carnegie-Mellon Institute, Pittsburgh, Pa. 15213.
25. E. Nembach: *J. Phys. Chem. of Solids,* 1968, vol. 29, pp. 1205-11.
26. R. A. Mercuri and J. M. Criscione: Union Carbide Corp., Carbon Products Div., Parma Technical Center, Parma, Ohio: Abstracts of Papers Presented at 158th National Meeting of the American Chemical Society, New York, 1969, vol. 158, Division of Inorganic Chemistry Abstract 33. A copy of the complete paper presented is available from the authors.
27. D. M. Poole and P. M. Martin: *Met. Rev.,* 1969, vol. 14, pp. 61-84.
28. E. M. Savitskii and M. A. Tylkina: *Rhenium,* B. W. Gonser, ed., pp. 67-83, Elsevier, New York, 1962.
29. D. E. Williams: LCR-2, A Fortran Lattice Constant Refinement Program, Ames Laboratory Report No. IS-1052, Iowa State University of Science and Technology, Ames, Iowa, November 1964.
30. *X-Ray Powder Data File, Amer. Soc. Testing Mater. Special Tech. Publi.* 48-J, J. V. Smith, ed., American Society for Testing Materials, Philadelphia, Pa., 1960; Re: No. 5-0702, 1953; Au: No. 4-0784, 1950.
31. T. F. Fedorov, E. I. Gladyshevskii, and L. V. Gorshkova: *Izv. Akad. Nauk SSSR, Metal.,* 1966, no. 6, pp. 134-36; English Abstract, *Russ. Met.,* 1966, no. 6, pp. 75-77.
32. L. V. Gorshkova, Yu. V. Voroshilov, and T. F. Fedorov: *Porosh. Met.,* 1969, no. 2, pp. 82-5; English translation, *Sov. Powder Met., Met. Ceram.,* 1969, no. 2, pp. 146-48.
33. S. S. Ordan'yan, N. V. Kosterova, and A. I. Avgustinik: *Izv. Akad. Nauk SSSR, Neorg. Mater.,* 1969, no. 5, pp. 389-90.
34. Yu. B. Kuz'ma, E. I. Gladyshevskii, L. V. Gorshkova, and T. F. Fedorov: *Diagrammy Sostoyaniya Metal. Sist., Mater. Vses. Soveschch.,* 1968, pp. 184-91.
35. L. V. Gorshkova, T. F. Fedorov, and Yu. B. Kuz'ma: *Porosh. Met.,* 1967, no. 4, pp. 42-45; English translation, *Sov. Powder Met., Met. Ceram.,* 1967, no. 4, pp. 287-90.
36. E. Stolz and K. Schubert: *Z. Metallk.,* 1962, vol. 53, pp. 433-44.
37. W. Rostoker and J. R. Dvorak: pp. 195-219, *Interpretation of Metallographic Structures,* Academic Press, New York, 1965.
38. K. Schubert, M. Balk, S. Bhan, H. Breimer, P. Esslinger, and E. Stolz: *Naturwiss.,* 1959, vol. 46, pp. 647-48.
39. E. K. Storms: *The Refractory Carbides,* Chap. II, III, V, VI, X, and XI, Academic Press, New York, 1967.
40. F. B. Baker, E. K. Storms, and C. E. Holley, Jr.: *J. Chem. Eng. Data,* 1969, vol. 14, pp. 244-46.
41. A. D. Mah: U. S. Bureau of Mines Rept. Invest. BM-RI-6518, 1964, 8 pp.
42. E. J. Huber, Jr. and C. E. Holley, Jr.: *J. Chem. Eng. Data,* 1968, vol. 13, pp. 252-53.
43. Ralph Hultgren, Pramod D. Desai, Donald T. Hawkins, Molly Gleiser, and Kenneth K. Kelley: *Selected Values of the Thermodynamic Properties of Metals and Alloys,* American Society for Metals, Metals Park, Ohio, to be published, fall 1972. Compilation dates: TaC, Dec. 1965; ThC and $ThC_{1.9}$, Dec. 1966; Uranium Carbides, Aug. 1967; and HfC, Feb. 1966.
44. E. J. Huber, Jr., C. E. Holley, Jr., and N. H. Krikorian: *J. Chem. Eng. Data,* 1968, vol. 13, pp. 253-56.
45. P. E. Potter: *J. Inorg. Nucl. Chem.,* 1969, vol. 31, pp. 1821-29.
46. E. K. Storms: *High Temp. Sci.,* 1971, vol. 3, pp. 99-122.
47. Gerald Stowe: Report to Professor L. Brewer for Chemistry course 106, University of California, Berkeley, California, 94720, June 2, 1965.
48. W. L. Worrell and Peter Meschter: School of Metallurgy and Mater. Sci., Univ. of Pennsylvania, Philadelphia, Pa., private communication, April, 1972.
49. Peter Ficalora: Dept. of Chem. Eng. and Metallurgy, Syracuse University, Syracuse, New York, 13210, private communication, August 1971.
50. R. S. Carbonara and G. D. Blue: *High Temp. Sci.,* 1971, vol. 3, pp. 225-30.
51. W. B. Pearson: *Handbook of Lattice Spacings and Structures of Metals* Vol. 2, Pergamon Press Inc., New York, 1967, pp. 1-4; 106 (Zr-Ag), 160 (Zr-Au), 300 (Zr-Ir), 349 (Zr-Os), 359 (Zr-Pd), 365 (Zr-Pt), 372 (Zr-Rh), 374 (Zr-Ru), 537 (Zr-Ag).
52. C. J. Raub and C. A. Anderson: *Z. Phys.,* 1963, vol. 175, pp. 105-14.
53. S. T. Zegler: *J. Phys. Chem. Solids,* 1965, vol. 26, pp. 1347-49.
54. A. Raman and K. Schubert: *Z. Metal.,* 1964, vol. 55, pp. 704-10.
55. M. V. Nevitt, J. W. Downey, and R. A. Morris: *Trans. TMS-AIME,* 1960, vol. 218, pp. 1019-23.
56. M. V. Nevitt: *Electronic Structure and Alloy Chemistry of the Transition Elements,* Paul A. Beck, ed., p. 134, Interscience Publishers, New York, 1963, Dover, N. Y., 1965.
57. N. Karlsson: *Acta Chem. Scand.,* 1952, vol. 6, pp. 1424-30.
58. J. O. Betterton, Jr. and D. S. Easton: *Trans. TMS-AIME,* 1958, vol. 212, pp. 470-75.
59. F. E. Wang: *J. Appl. Phys.,* 1967, vol. 38, pp. 822-24; (with D. W. Ernst) 1968, vol. 39, pp. 2192-95; (with Y. Chueng, K. Hu, and P. Tsao) 1969, vol. 40, pp. 1980-83.
60. L. Kaufman: Manlabs, Cambridge, Mass., private communication, August 18, 1966; L. Kaufman and H. Bernstein: *Computer Calculation of Phase Diagrams,* Academic Press, New York, 1970.
61. N. H. Krikorian, T. C. Wallace, M. C. Krupka, and C. L. Radosevich: *J. Nucl. Mater.,* 1967, vol. 21, pp. 236-38.
62. E. Raub and G. Falkenburg: *Z. Metallk.,* 1964, vol. 55, pp. 190-92.
63. Peter Riessenfeldt: Report to Professor L. Brewer for Chemistry course 106, University of California Berkeley, California 94720, 1966.
64. N. H. Krikorian: *J. Less-Common Metals,* 1971, vol. 23, pp. 271-79.
65. E. D. Eastman, Leo Brewer, LeRoy A. Bromley, Paul W. Gilles, and Norman L. Lofgren: *J. Amer. Ceram. Soc.,* 1951, vol. 34, pp. 128-34.
66. M. W. Evans: pp. 312-20, *The Chemistry and Metallurgy of Miscellaneous Materials: Thermodynamics,* L. L. Quill, ed., National Nuclear Energy Series, Manhattan Project Technical Section, Division IV – Plutonium Project Record, vol. 19B, McGraw-Hill, New York, 1950.
67. R. L. Montgomery: Bureau of Mines, R. I. 6146, 1962, pp. 1-9.
68. H. Holleck and H. Kleykamp: *J. Nucl. Mater.,* 1970, vol. 35, pp. 158-66.
69. G. M. Campbell, L. J. Mullins, and J. A. Leary: *Thermodyn. Nucl. Mater., Proc. Symp., Vienna 1967,* pp. 75-88, Int. At. Energy Agency, Vienna, Austria, 1968.
70. W. Bronger and W. Klemm: *Z. Anorg. Chem.,* 1962, vol. 319, pp. 58-81. Note: Reactions 1 and 2, pg. 59 are not balanced.
71. E. Raub and E. Röschel: *Z. Metallk.,* 1953, vol. 54, pp. 455-62.
72. A. E. Dwight: *Trans. TMS-AIME,* 1959, vol. 215, pp. 283-86.
73. J. H. Wallbaum: *Naturwiss.,* 1952, vol. 30, p. 149.
74. A. E. Dwight and P. A. Beck: *Trans. TMS-AIME,* 1959, vol. 215, pp. 976-79.
75. C. B. Alcock and P. Grieveson: *J. Inst. Metals,* 1962, vol. 90, pp. 304-10.
76. T. K. Biswas and K. Schubert: *Z. Metallk.,* 1967, vol. 58, pp. 558-59.
77. A. E. Dwight: *Trans. ASM,* 1961, vol. 53, pp. 479-500.
78. P. R. Wengert and L. Spanoudis: private communication, March 15, 1972.
79. M. V. Nevitt and J. W. Downey: *Trans. TMS-AIME,* 1962, vol. 224, pp. 195-
80. K. Schubert, S. Bhan, W. Burkhardt, R. Gohle, H. G. Meissner, M. Potzschke, and E. Stolz: *Naturwiss.,* 1960, vol. 47, p. 303.

81. M. Norman and I. R. Harris: *J. Less-Common Metals,* 1969, vol. 18, pp. 333-45.
82. A. E. Dwight, R. A. Conner, Jr., and J. W. Downey: *Acta Cryst.,* 1965, vol. 18, pp. 835-39.
83. H. J. Wallbaum: *Naturwiss.,* 1943, vol. 31, pp. 91-92.
84. K. Schubert, S. Bhan, T. K. Biswa, K. Frank, and P. K. Panday: *Naturwiss.,* 1968, vol. 55, pp. 542-43.
85. P. Krautwasser, S. Bhan, and K. Schubert: *Z. Metallk.,* 1968, vol. 59, pp. 724-29.
86. E. Raub and M. Engel: *Z. Metallk.,* 1948, vol. 39, pp. 172-77.
87. M. V. Nevitt: *Trans. TMS-AIME,* 1958, vol. 212, pp. 350-55.
88. A. S. Darling, G. L. Selman, and R. Rushforth: *Platinum Metals Rev.,* 1970, vol. 14, pp. 124-30.
89. L. S. Darken and R. W. Gurry: *Physical Chemistry of Metals,* McGraw-Hill, New York, 1953.
90. N. L. Pravoverov and Yu. G. Kolonin: *Izv. Akad. Nauk SSR, Metally,* 1969, no. 2, pp. 188-90; English translation, *Russ. Met.,* 1969, no. 2, pp. 154-55.
91. M. Hoch, E. F. Juenke, and L. H. Sjodahl: *Thermodyn. Nucl. Mater., Proc. Symp., Vienna 1967,* pp. 497-510, Int. At. Energy Agency, Vienna, Austria, 1968.
92. K. Anderko: *Z. Metallk.,* 1959, vol. 50, pp. 681-6.
93. B. Erdman and C. Keller: *Inorg. Nucl. Chem. Lett.,* 1971, vol. 7, pp. 675-83.
94. V. N. Eremenko, T. D. Shtepa, and E. L. Semenova: *Dopov. Akad. Nauk Ukr. RSR,* 1972, Ser. B, vol. 34, pp. 50-52.